

Torsional Force Microscopy of Van der Waals Moirés and Atomic Lattices

Mihir Pendharkar,^{1, 2,*} Steven J. Tran,^{1, 3} Gregory Zaborski Jr.,^{1, 2} Joe Finney,^{1, 3}
 Aaron L. Sharpe,⁴ Rupini V. Kamat,^{1, 3} Sandesh S. Kalantre,^{1, 3} Marisa Hocking,^{1, 2}
 Nathan J. Bittner,⁵ Kenji Watanabe,⁶ Takashi Taniguchi,⁷ Bede Pittenger,⁸ Christina J. Newcomb,⁹
 Marc A. Kastner,^{1, 3, 10} Andrew J. Mannix,^{1, 2} and David Goldhaber-Gordon^{1, 3, †}

¹Stanford Institute for Materials and Energy Sciences,

SLAC National Accelerator Laboratory, Menlo Park, CA 94025

²Department of Materials Science and Engineering, Stanford University, Stanford, CA 94305

³Department of Physics, Stanford University, Stanford, CA 94305

⁴Materials Physics Department, Sandia National Laboratories, Livermore, CA 94550

⁵Independent Researcher

⁶Research Center for Electronic and Optical Materials,

National Institute for Materials Science, 1-1 Namiki, Tsukuba 305-0044, Japan

⁷Research Center for Materials Nanoarchitectonics,

National Institute for Materials Science, 1-1 Namiki, Tsukuba 305-0044, Japan

⁸Bruker Nano Surfaces, AFM Unit, Santa Barbara, CA 93117

⁹Stanford Nano Shared Facilities, Stanford University, Stanford, CA 94305

¹⁰Department of Physics, Massachusetts Institute of Technology, Cambridge, MA 02139

(Dated: 16 August 2023)

In a stack of atomically-thin Van der Waals layers, introducing interlayer twist creates a moiré superlattice whose period is a function of twist angle. Changes in that twist angle of even hundredths of a degree can dramatically transform the system's electronic properties. Setting a precise and uniform twist angle for a stack remains difficult, hence determining that twist angle and mapping its spatial variation is very important. Techniques have emerged to do this by imaging the moiré, but most of these require sophisticated infrastructure, time-consuming sample preparation beyond stack synthesis, or both. In this work, we show that Torsional Force Microscopy (TFM), a scanning probe technique sensitive to dynamic friction, can reveal surface and shallow subsurface structure of Van der Waals stacks on multiple length scales: the moirés formed between bi-layers of graphene and between graphene and hexagonal boron nitride (hBN), and also the atomic crystal lattices of graphene and hBN. In TFM, torsional motion of an AFM cantilever is monitored as it is actively driven at a torsional resonance while a feedback loop maintains contact at a set force with the surface of a sample. TFM works at room temperature in air, with no need for an electrical bias between the tip and the sample, making it applicable to a wide array of samples. It should enable determination of precise structural information including twist angles and strain in moiré superlattices and crystallographic orientation of VdW flakes to support predictable moiré heterostructure fabrication.

Introduction

The theoretical prediction of electronic Bloch bands in moiré superlattices in twisted Van der Waals (VdW) bilayers [1–5] and the subsequent observations of a correlated insulator state and unconventional superconductivity in magic-angle twisted bilayer graphene (tBG) [6, 7] have unlocked a powerful new approach to tuning and discovering electronic properties of materials. tBG has displayed topological effects (orbital ferromagnetism [8] and quantized anomalous hall effect [9]), ferroelectricity [10], strange-metal behavior [11, 12], and more depending on interlayer twist angle, applied electric and magnetic fields, and other subtle structural features. For example, orbital ferromagnetism in tBG appears to depend on not only the twist between the two layers of graphene but also the twist between graphene and encapsulating hexagonal boron nitride (hBN) [13]. Uniaxial strain has recently been found to dramatically influence electronic properties of tBG away from magic angle [14, 15]. Beyond tBG, a burgeoning array of

moiré systems, extending to more layers and different constituent layers, also show exciting behaviors. Unfortunately, moiré superlattices based on 2D materials are plagued by poor control, reproducibility, and spatial uniformity of twist angle and other structural properties [16]. Convenient, rapid, and reliable techniques for imaging moiré superlattices will be needed to provide feedback to guide improvements in heterostructure synthesis.

Priorities for capabilities of such a technique should include: 1) imaging moiré superlattices on the scale of individual unit cells (ranging from nanometers to microns), 2) imaging over large areas (microns), 3) imaging subsurface moiré superlattices and 4) imaging atomic crystal lattices of VdW materials (sub-nanometer). This covers many but not all structural properties known to strongly influence electronic properties. As has been succinctly summarized by McGilly *et al.* [17], and is still true, techniques that depend on cryogenics, ultra-high vacuum, complex infrastructure, restrictive environmental controls and/or extensive sample preprocessing (in-

cluding nanofabrication) can provide powerful information but are not appropriate for quick feedback to stack synthesis. Instead we should seek a technique that is “straightforward”: operating in air, at room temperature. To allow characterizing partially-complete stacks, the technique should not require electrical contacts or modifications to the sample or its surface, and should work on VdW stacks on soft polymers commonly used as stamps for stack assembly. Here we aim to address the need for such a rapid feedback technique.

Multiple scanning probe techniques have recently been shown to provide structural information on moirés. Among those, some can be used in air at room temperature, often on a commercial AFM platform, offering the promise of tight feedback for heterostructure synthesis. Conductive AFM (C-AFM) can image atomic lattices [18], provided an electrical contact is made to a conductive sample or a conductive substrate below an atomically-thin insulating sample. Simple tapping-mode AFM can image open-face graphene-hBN moirés and few-nanometer-deep hBN-hBN moirés with remarkable few-nanometer lateral resolution over microns [19]. To our knowledge this approach has not yet worked for tBG, nor has atomic-scale imaging been shown in ambient on atomically-thin stacks. Scanning Microwave Impedance Microscopy (s-MIM) has imaged open-face tBG moirés under ambient conditions [20, 21]. Although it does not require an electrical sample contact, it does require specialized hardware and has not been shown to resolve atomic lattices. Lateral (or Friction) Force Microscopy (LFM/FFM), a variation of contact AFM focusing on lateral rather than vertical tip deflection has perhaps come the closest to providing a facile method for mapping structural features at both moiré scale [22, 23] and atomic lattice scale on hBN and graphite [24, 25]: evidently lateral friction forces vary with tiny changes in the positioning of the tip on the sample. This method satisfies most of the criteria laid out above but has not been shown to resolve subsurface moirés, to our knowledge.

Piezoresponse force microscopy (PFM), a contact AFM technique, has produced remarkable maps of moirés with few-nanometer resolution over hundreds of nanometers [17]. By superimposing two orthogonal scans, taken by rotating the sample by 90°, the full hexagonal unit cell of a tBG moiré has been imaged. Subsurface moirés were also observed, though atomic lattices have not been. The authors shared their surprise that this technique would give contrast on moiré samples, especially tBG which lacks the inversion asymmetry necessary to generate a piezo-electric response [17, 26, 27]. Though PFM is expected to require closing an electrical loop between the AFM tip and the sample, published studies suggest that PFM in fact resolves the moiré contrast even on insulating substrates. In attempting to replicate the beautiful maps achieved by this technique, we stumbled upon torsional resonances, sensitive to dynamic friction at the

AFM tip-sample interface, as being central to resolving moiré contrast.

Experimental

In this work, we map spatial variations in torsional resonances of an AFM cantilever, in a technique we term Torsional Force Microscopy (TFM). Fig. 1(A) presents a schematic diagram of the key components that enable TFM. The basic operation of TFM can be divided into two parts: first, a closed loop feedback (routed in purple arrows in Fig. 1(A)) tracks the topography to maintain a set vertical loading force; second, a torsional resonance is excited in the AFM cantilever and the mechanical response is measured in open loop (green arrows in Fig. 1(A)). The first closed feedback loop is identical to that used in contact AFM, LFM, or PFM, while the second open loop shares similarities with non-contact or tapping-mode AFM. The two loops operate in parallel. TFM does not require any electrical connections to either the tip or the sample, so the two can be electrically floating and insulating.

The bending of the cantilever as it moves into contact with the sample surface is measured as a change in the vertical position of the laser spot on a four-quadrant position sensitive photodetector. Such a photodetector provides outputs proportional to the position of the laser spot along the vertical and horizontal axes. Thermal or mechanical drift and bimetallic expansion of coated AFM tips under the incident laser led to force offsets of the order of hundreds of nanonewtons over a few hours after aligning the laser on the cantilever. This drift, if not periodically checked and corrected, can damage both the AFM tip and the sample. We developed a protocol to accurately estimate the force applied by the AFM tip on the sample surface (see supplementary materials).

In parallel to the closed feedback loop, an independent open loop maps spatial variation in the frictional response, revealing both moiré superlattices and atomic lattices. This open loop operates by mechanically exciting a torsional motion of the AFM cantilever, near a torsional resonance. Two piezos in the cantilever holder are driven 180° out of phase with each other, to specifically excite torsional motion (Fig. 1(A).) This mechanical excitation of torsional resonance modes was pioneered by L. Huang & C. Su [28, 29]. By sweeping torsional drive frequency, maxima in signal amplitude consistent with torsional modes of the AFM cantilever are measured (as an AC voltage) on the lateral deflection channel of the photodetector. The amplitude of this lateral signal in volts can be used to deduce the amplitude of torsional motion of the cantilever in nanometers, in turn enabling deduction of a lateral force - orthogonal to the vertical loading force [30].

Fig. 1(B) shows the thermal resonance spectrum (without any mechanical excitation) of an AFM cantilever measured in air at room temperature, far from any sur-

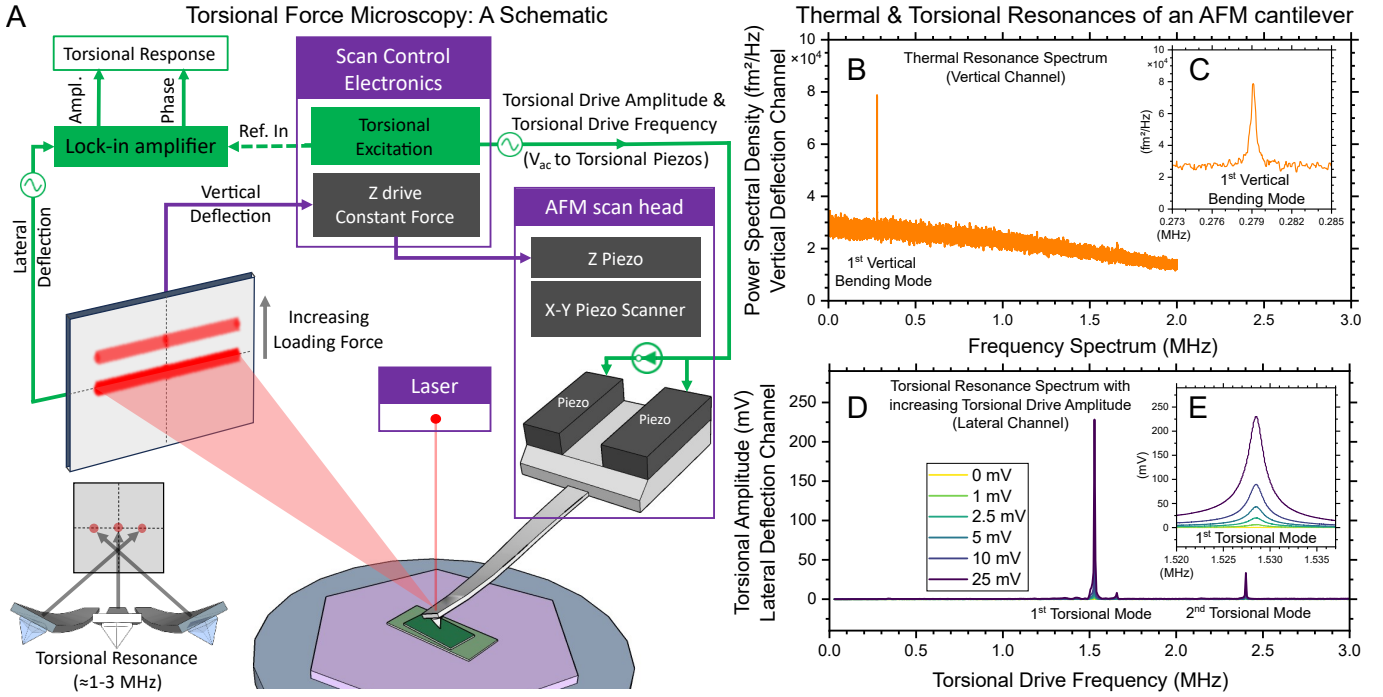


FIG. 1. Torsional Force Microscopy (TFM) (A) Schematic diagram of TFM in a system with mechanically driven torsional resonances. An incident laser beam reflects off an AFM cantilever that is driven at a torsional resonance (typically 1 to 3 MHz). This torsional resonance is mechanically excited by applying an AC drive voltage to two piezos mounted in the AFM probe holder. We measure the amplitude and phase of the resulting lateral deflection signal on the photo-detector. A constant vertical loading force between the AFM tip and the imaging surface is maintained by a feedback loop that moves the AFM tip up and down according to the topography, as in contact-AFM. (B) Thermally-excited resonance of an AFM cantilever (nominal spring constant 42 N/m) at room temperature in air, far from any surface, in ambient light, without any mechanical drive. The only measurable peak in power spectral density of the vertical deflection channel of the photo-detector is the fundamental resonance, i.e. the first vertical bending mode of the cantilever. (C) Zooming into a narrower frequency range shows that the resonance is at 279 kHz. (D) Torsional response of the same AFM cantilever (lateral photo-detector channel) as a function of drive frequency of the torsional piezos, for several drive amplitudes. Two prominent resonances appear at 1.529 MHz (E) and at 2.4 MHz, respectively.

face, on the vertical deflection channel of the photodetector. Inset in Fig. 1(C) shows the first vertical bending mode of the AFM cantilever with a peak at 279 kHz. When the torsional frequency spectrum is measured on the same cantilever, two resonances appear at 1.529 MHz and 2.4 MHz, as shown in Fig. 1(D). The presence of torsional modes at frequencies much higher than the first vertical bending mode is expected, with the first mode typically appearing between 1 to 1.6 MHz and the second between 1.4 to 3 MHz. Cantilevers of different geometries may behave differently and it is possible that only one of these two prominent resonances is the torsional mode while the other is a lateral bending mode [29, 31]. The torsional amplitude measured at the photodetector grows linearly with piezo drive amplitude (Fig. 1(E)). For this AFM cantilever, a torsional resonance amplitude of 225 mV is measured for a 25 mV torsional drive amplitude. Typically, the resonance with the highest ratio of response to drive was chosen for imaging, though for the few instances when the second most prominent resonance was chosen, suitable results were still obtained.

A lock-in amplifier operating near the torsional drive frequency demodulates the measured torsional amplitude and phase at every pixel. Typical line scan speeds (each line consisting of both trace and retrace) ranged from 2 Hz over microns, to 4 Hz over hundreds of nanometers and 30 Hz over tens of nanometers. At these speeds, the lock-in amplifier input bandwidth was typically set between the lower end of 0.211 kHz (limited by electronics) to 10 kHz, with increasing bandwidth at increasing speeds, to avoid digitization. A standard operating procedure (SOP) to set up TFM is provided in the supplementary materials.

It is necessary to make a distinction between Torsional Force Microscopy (TFM) and Torsional Resonance Microscopy (TRM). As laid out by L. Huang and C. Su, torsional resonance microscopy feeds back on the torsional resonance amplitude and uses the deviation in this amplitude from its setpoint to move the Z-piezo, thus varying the vertical loading force [28]. We found that rapidly varying the vertical loading force was not ideal for imaging atomically thin materials placed on soft polymer

stamps (i.e. surfaces that risk being torn under excessive forces), though TRM may be suitable for other applications. A phase-locked loop (PLL)-guided frequency modulation TRM, tracking the torsional resonance frequency as it shifts due to interaction with the sample, may be an alternative and has been demonstrated [32].

Results

We now employ TFM to study a common VdW heterostructure of graphene on hBN. This sample was prepared in vacuum by picking up an exfoliated flake of hBN followed by graphene. Fig. 2(A) shows an optical microscope image of this open-face heterostructure. Fig. 2(B) shows the honeycomb atomic lattice of hBN as imaged by TFM. The atomic lattice could be measured with both the first and the second torsional resonances. Remarkably, commonly-available AFM cantilevers (ra-

dius ≤ 25 nm) could be used without the need for sharp AFM tips, though sharp tips were preferred (radius ≤ 10 nm). To counter the effects of thermal drift, piezo creep, and piezo hysteresis, fast line scan speeds of between 10-30 Hz were used over square areas typically between 4 to 20 nm on a side. Extending the piezo scanning distance along the fast scan axis by 10% beyond the edge of the frame reduced the distortion in images. It is unclear whether the features correspond to true atomic resolution versus atomic lattice resolution (i.e., spatially averaged, eggcarton-on-eggcarton tip-sample interaction) [33]. In any case, the ability to easily visualize the atomic crystal lattice in air at room temperature in a commercially available AFM has substantial implications for guiding stacking of atomically thin materials.

Fig. 2(C) shows TFM of a moiré superlattice formed between monolayer graphene and hBN with a period of a mere 2.6 nm. Here and throughout this manuscript, reported moiré periods are extracted from 2D FFTs. The clarity of the image highlights the impressive lateral resolution of TFM. Upon further zooming into the moiré structure, a periodicity consistent with the atomic lattice of either graphene or hBN emerged, superimposed on the moiré superlattice (see Fig. 2(D)). Supplementary Fig. S2 shows the complementary TFM amplitude and phase images of Fig. 2. As the AFM tip is in direct contact with graphene while taking this image, the prominent atomic lattice is likely that of graphene. However, the vertical loading is sufficient that the underlying hBN lattice might be imaged. In addition to demonstrating the success of TFM in imaging the atomic crystal lattices of hBN and graphene, this result also confirms the sensitivity of TFM to moiré superlattices formed at the interface of monolayer graphene and hBN.

Next, we image a moiré superlattice formed in tBG. To establish reproducible conditions for imaging regardless of the AFM tip used, the sample being imaged, or other variables, Fig. 3 examines the impact of two key parameters of TFM: loading force and torsional drive amplitude. These two variables in turn control the tip-sample interaction. The tBG-on-hBN open-face heterostructure was prepared in vacuum, with an intended tBG twist angle of 2°. The period of the imaged moiré superlattice corresponds to a twist of 1.88°.

Moiré superlattices in tBG imaged using contact AFM techniques such as PFM and LFM have typically been reported for forces of 20-50 nN [17, 23]. To study the impact of loading force, an accurate knowledge of the force applied is necessary (especially at low forces). We develop a protocol to accurately determine the force, starting by determining the minimum force required to keep the tip in contact with the sample. We refer to this baseline as “Contact + 0 nN”. Fig. 3(A-E) show a schematic and then TFM images acquired as increasing force from “Contact + 0 nN” to 150 nN in steps of 50 nN, at a constant torsional drive amplitude of 2.5 mV. Moiré contrast

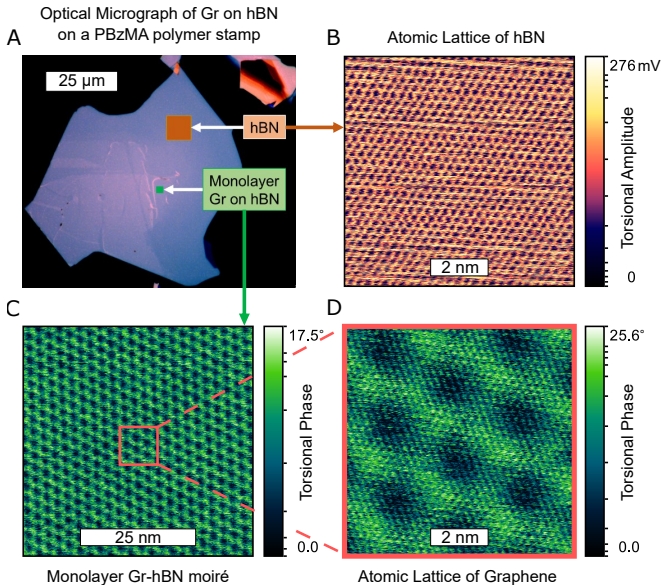


FIG. 2. Torsional Force Microscopy of the Atomic Lattice of hBN & Graphene & of a moiré of Monolayer Graphene on hBN (A) Optical microscope image of a Graphene-hBN heterostructure on a multilayer polymer stamp. Color scale is adjusted to highlight the contrast between graphene and hBN. (B) TFM image taken at the approximate location of hBN marked in (A) shows torsional amplitude revealing the atomic lattice of hBN, at a force of 50 nN and a torsional drive of 2.5 mV at a speed of 24.4 Hz per line. (C) Moiré superlattice formed between monolayer graphene and hBN, measured at the approximate location marked in (A). A moiré period of 2.6 nm indicates a relative twist between monolayer graphene and hBN of 5.4°. (D) Higher resolution image taken from the center of (C). The fine granular features of the moiré in (D) are likely the underlying lattice of graphene. (C,D) were imaged at a force 100 nN and a torsional drive of 5 mV at a speed of 8.14 Hz per line. (B,C,D) were imaged with a 16x lateral signal amplifier enabled and at the 1.428 MHz torsional resonance, at a scan angle of 90°.

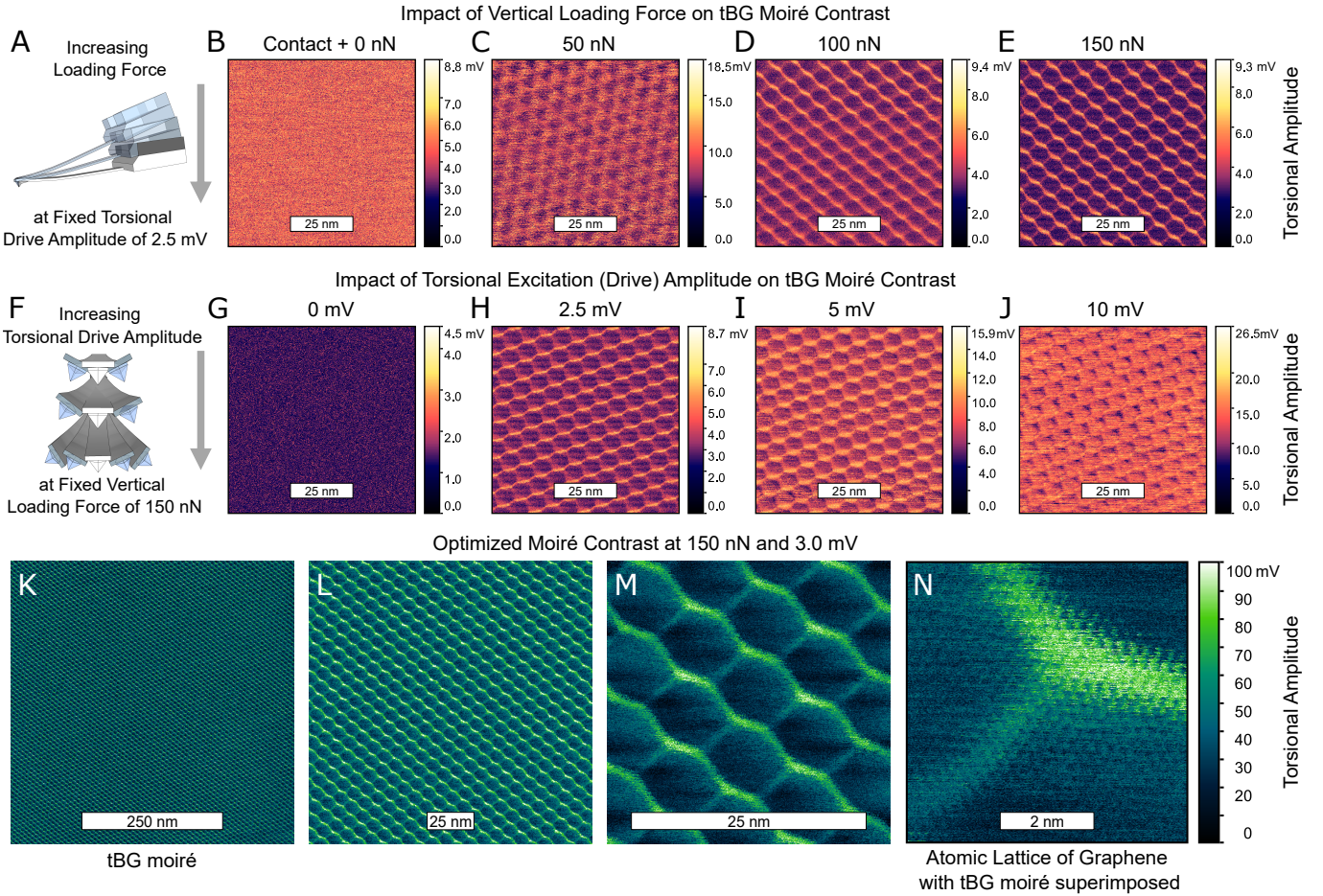


FIG. 3. Imaging moirés in tBG: Impact of Vertical Loading Force & Resonant Torsional Excitation Amplitude on moiré contrast (A) Schematic of increasing vertical loading force at a fixed torsional excitation. (B-E) TFM maps on the surface of tBG as force is increased from the minimum required to maintain contact of the AFM tip with the sample surface (Contact + 0 nN) to 150 nN in steps of 50 nN. A moiré superlattice is not visible at the lowest force but becomes stronger in contrast as force is increased. (F) Schematic of increasing torsional excitation amplitude at a fixed vertical loading force. (G-J) TFM maps with torsional drive amplitude increased from 0 to 10 mV. Though no moiré is observed at 0 mV, a moiré is clearly observed at 2.5 mV. Upon further increasing the drive amplitude the moiré persists but the contrast in torsional amplitude decreases, instead appearing as a change in torsional phase (see supplementary Fig.S3). (K) Using the near-optimal imaging parameters now determined for TFM, we image a larger region, revealing a moiré superlattice across 500x500 nm. The moiré period of 7.5 nm corresponds to a twist in tBG of 1.88°. (L,M,N) Subsequent images taken at higher resolution near the center of (K). (M) shows a fine granular detail accompanying the moiré which is revealed in (N) to resemble an atomic lattice, most likely of the uppermost graphene surface in contact with the AFM tip, with the tBG moiré superimposed. (B-E, G-J) were imaged at 1.4568 MHz with the lock-in amplifier bandwidth set to 102.6 kHz to ensure the resonance frequency was always within the input bandwidth. (K-N) were imaged at 1.4576 MHz, the peak of torsional resonance at 150 nN and at 3 mV drive amplitude, with the lock-in amplifier bandwidth reduced to 2 kHz and a 16x lateral signal amplifier enabled. (B-E, G-J, K-N) were all imaged at 4.07 Hz line scan speed and a scan angle of 90°.

increases dramatically as force is increased. Next, the torsional excitation's drive amplitude is increased, while keeping the drive frequency and force fixed. Though some torsional excitation is necessary, high contrast in measured signal amplitude is immediately apparent at very low drive amplitude. As drive amplitude is increased, the measured signal switches from amplitude to phase. The mechanism for this remains to be studied.

A force of 150 nN was not required on all tBG samples; moiré superlattices in tBG were successfully imaged

at forces from 10 nN to 300 nN. Fresh AFM tips on fresh samples enabled mapping moiré superlattices at comparatively lower forces. With a sharp tip apex of a fresh tip, the pressure applied on the surface is likely much greater for a given force, so we speculate that the moiré contrast depends directly on the pressure applied, rather than the force. Samples likely accumulate a stubborn layer of adsorbates over months demanding higher forces for imaging through these layers. The tBG sample imaged in Fig. 3 was prepared over five months prior to be-

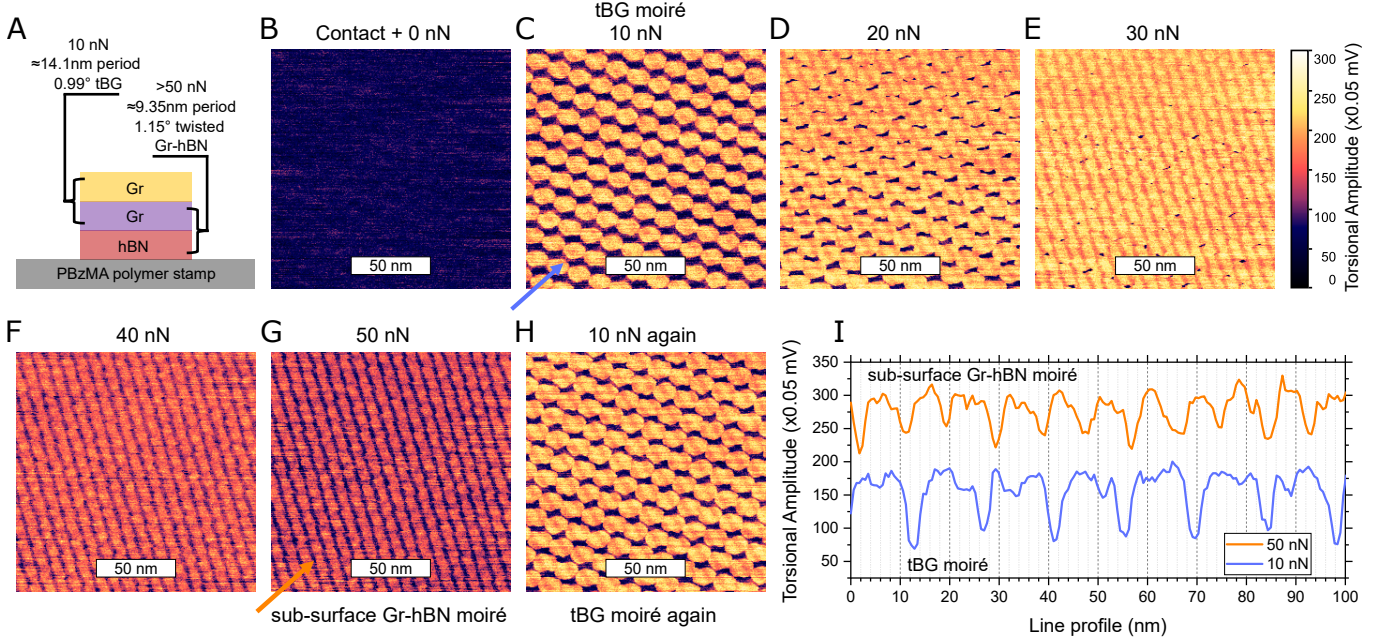


FIG. 4. Imaging a subsurface moiré (A) Schematic layer structure of the sample being imaged: tBG is stacked atop a flake of hBN on a multi-layer polymer stamp terminated with PBzMA. (B-H) are all imaged at the same location of the sample. (B) Resonant torsional amplitude at a vertical force equivalent to the minimum force required for the AFM tip to remain in contact with the surface (Contact + 0 nN). (C) Increasing the force to 10 nN reveals a well-defined moiré pattern with a period of 14.1 nm. (D-F) reveal a transition from the moiré observed in (C) to a moiré in (G) as force is stepped by 10 nN with each image. The moiré period observed in (G) at a force of 50 nN is 9.35 nm, different from the observed period in (C) at a force of 10 nN. (H) When force is reduced back down to 10 nN, the pattern returns to resembling that in (C), indicating the change in moiré from (C) to (G) is not a temporary surface cleaning effect. (I) Line profiles, taken along lines indicated by the blue (C) and orange (G) arrows. The low-force moiré is likely to be a tBG moiré. As force is increased, it is likely that the moiré formed by the subsurface graphene with the underlying hBN is revealed. The period of 14.1 nm of the tBG moiré corresponds to a twist angle of 0.99°. The period of 9.35 nm of the Gr-hBN moiré corresponds to a twist angle of 1.15°. These moiré periods are extracted from 2D FFT of the image and not their line profiles. All images in the series were acquired at the 1.3299 MHz resonance at 0.5 Hz line scan speed at a scan angle of 0°, with the 16x lateral signal amplifier enabled. The torsional piezos were driven indirectly by crosstalk in the electronics by applying 500 mV drive amplitude - which would correspond to 10-12.5 mV of torsional drive amplitude applied directly to the piezos. 10 nN and 50 nN line profiles are offset for clarity.

ing imaged. It was mainly stored in a nitrogen drybox, but was exposed to air for days at a time on multiple occasions.

As the force was increased from zero (not in contact with the sample) to the minimum required to remain in contact (“Contact + 0 nN”) and onward to hundreds of nanonewtons, the torsional resonant modes were observed to shift to higher frequencies. The measured amplitude of the resonance also reduced with increasing force, indicating damping of the resonance [29]. The shift in frequency ranged from tens of Hz to tens of kHz depending on the force applied.

Once optimal parameters of force and drive amplitude were determined, the moiré superlattice in tBG was imaged at varying length scales. The lock-in amplifier bandwidth was also reduced to improve SNR. Fig. 3(K-N) show a tBG moiré with a period of 7.5 nm, imaged with successively reduced scan area is sequentially reduced without changing any other settings. The smallest-scale map (N) covers portions of three moiré cells; superim-

posed on this moiré pattern is an atomic-scale periodic structure, likely the atomic lattice of graphene. These results point to the versatility of TFM in imaging both moiré superlattices and atomic lattices on the same sample, without having to change anything more than the frame size. Supplementary Fig. S3 shows TFM phase images corresponding to the amplitude images of Fig. 3.

Going forward, we continued to follow this protocol of first determining the minimum force required to remain in contact and then stepping up from “Contact + 0 nN” to higher forces until satisfactory moiré contrast is observed.

For one sample of tBG on hBN (schematic cross-section, Fig. 4(A)), the moiré superlattice observed at 10 nN (Fig. 4(B)) dramatically transformed as force was stepped up to 50 nN (C-G). Upon lowering the force back to 10 nN (H), the moiré returned to resemble the pattern observed at 10 nN prior to the force ramp. Line profiles (I) along arrows marked in (C) and (G) show two different periods for these images, suggesting that changing

the applied force allows us to select which of two superimposed moirés to image.

The moiré seen at low applied force is likely that of tBG, whereas the moiré seen at high force is likely below the surface, presumably from unintentional rotational near-alignment of graphene on hBN. The period of the first moiré is 14.1 nm, corresponding to tBG twisted at 0.99°. This should be compared to the 1.3° intended fabricated twist angle of the tBG. A twist relaxation of 0.3° is often seen at these low twist angles [34–36]. The subsurface moiré period of 9.35 nm corresponds to a graphene-hBN moiré at 1.15° twist. These results indicate that increasing force non-destructively allows TFM to map a subsurface moiré. On many additional tBG samples, we have now seen a second moiré corresponding to an underlying hBN’s near-alignment to the subsurface layer of graphene.

This measurement was performed before we understood the mechanism for TFM imaging and the measurement was set up with excitation routed to the AFM tip, as is common in modes like PFM. We later found that due to crosstalk, torsional piezos in the probe holder were driven with an excitation 2-2.5% of the amplitude applied to the AFM tip, and that the AFM tip was disconnected from the electrical circuit. A detailed description of this issue and a comparison of the frequency spectrum in TFM mode (directly-driven torsional piezos) vs PFM mode (crosstalk-driven torsional piezos) is shown in supplementary Fig. S1.

Fig. S5 shows a $2 \times 2 \mu\text{m}$ map of a tBG moiré with a spatially-varying period of 44-51 nm, corresponding to twist angles around 0.3°, demonstrating that TFM can image nanometer-scale moirés over areas relevant to typical electronic devices. The moiré unit cells appear hexagonal, suggesting that the surface is unreconstructed despite the small twist angle [37, 38], though it is possible that TFM is not sensitive to the internal structure of the moiré unit cell. Though we mostly studied stacks made in vacuum, we also confirmed that TFM works on tBG-hBN samples prepared in air on PC stamps (Fig. S6).

Discussion

We now examine the origin of both moiré and atomic lattice contrast in TFM. In LFM, a more commonly-used technique, the AFM cantilever’s lateral deflection is measured on the photodetector as the tip is dragged along the surface. In TFM the tip again rubs against the sample surface, now at a drive frequency near the MHz resonance of the cantilever, and changes in the resonant response are measured on the photodetector. By analogy we suggest that the signal on the photodetector in TFM is a measure of tip-sample friction, as in LFM. This view is supported by our observation of increasing contrast with increasing vertical tip-sample force. Moiré contrast originating from friction has been reported to be velocity-dependent, so the higher tip-sample veloci-

ties in TFM may provide higher contrast for imaging 2D materials [39].

Though both the atomic lattice of VdW materials and their moirés have also been imaged with LFM [22], TFM offers several advantages. First, TFM adds the ability to image subsurface moiré superlattices. Second, like other finite-frequency techniques TFM is resilient to electronic noise outside of the lock-in amplifier’s input bandwidth. In comparison, LFM and contact AFM operate by summing the signal from DC to a few kHz (limited by a low pass filter) and are therefore strongly affected by 1/f noise. Third, TFM can work with a wide range of cantilevers, allowing applying high vertical forces where needed to enhance moiré visibility. LFM by contrast uses cantilevers with a very low spring constant ($\ll 0.5 \text{ N/m}$), limiting the range of vertical forces that can be applied. Lastly, we have found that TFM can yield good contrast at any scan angle relative to the long axis of the cantilever (Fig. 2 and Fig. 3 used 90° scan angle, and Fig. 4 used 0°) whereas LFM requires imaging at a fixed scan angle of 90°.

Next, we compare TFM with lateral PFM at contact resonance (or CR-PFM). Here as well, TFM offers several advantages. First, TFM can image a tBG moiré in a single 2-dimensional scan. In contrast, CR-PFM has been reported to require superimposing two orthogonal images, with manual rotation of the sample in-between, to fully resolve the hexagonal unit cell of a large-period moiré superlattice. Secondly, TFM can image atomic lattices, which has not yet been reported for PFM. Lastly, TFM does not require a conducting AFM tip with bias applied between the tip and the sample, which PFM does require.

To implement TFM in instruments lacking the capability for mechanically exciting torsional resonances in an AFM cantilever, photothermal excitation of torsional resonances has recently been demonstrated [40].

Despite TFM’s many advantages, there remains a key drawback that must also be acknowledged. Increasing moiré contrast requires increasing force. Excessive force can damage sensitive samples. Operating with high torsional drive amplitude at low forces and tracking frequency shift with a PLL, to image dynamic friction at the tip-sample interface, may be a potential workaround but remains to be extensively tested.

TFM also shares issues faced by other ambient-based scanning probe techniques: thermal drift, piezo creep and piezo hysteresis in the lateral (X-Y) scan axis, which reduce accuracy and precision of quantitative extraction of moiré period and thus twist angle and strain. Temperature- and humidity-controlled enclosures, as well as correcting for piezo creep and hysteresis (either actively during imaging or using sensor data post-imaging), should help reduce these errors. Additionally, with the difference between the lattice constants of hBN and graphene being within the calibration uncertainty for am-

bient scanning probe techniques, TFM alone cannot be used to identify which atomic lattice is being imaged –prior knowledge of the structure studied, or access to other probes, is necessary. Similarly, twist relaxation as well as unintentional deviation from the fabricated twist angle in tBG on hBN stacks makes attribution of the moiré observed to either of the two possible moiré systems (tBG or Gr-hBN), challenging, especially if only one moiré, of period less than 14.25 nm, has been observed.

Conclusion

An open secret in the field of VdW materials is the poor success rate of most scanning probe techniques at imaging moiré superlattices formed in tBG –a problem not shared with the moirés formed in Gr-hBN, which can be imaged rather easily in conventional tapping-mode AFM. Using the SOP developed for TFM we were able to find at least one moiré in 94% of the 33 regions in 32 unique samples measured. Regions that did not show a moiré had likely relaxed to bernal stacking. Atomic lattices were observed at an even higher success rate (see supplementary note on duration and volume of study).

To summarize, torsional force microscopy enables non-destructive imaging of atomic crystal lattices and of moiré superlattices formed in VdW materials, in air at room temperature. Relying on dynamic friction at the tip-sample interface, with detection sensitivity enhanced by the torsional resonance of the AFM cantilever, TFM operates without the need for any electrical contacts to either the sample or the AFM tip. Thus TFM can be applied to give tight feedback on the structure of synthesized VdW stacks, helping make such synthesis more controlled. Given the strong dependence of electronic band structure on the interlayer twist angle and its spatial variation, this could have a transformative impact on fundamental and applied research on VdW materials and devices.

Sample preparation & AFM measurements

Samples prepared in vacuum as part of this work used a robotic vacuum stacking tool based on one previously developed by one of the authors [41]. Imaging was performed with the stack placed on a PBzMA terminated multi-composition polymer stamp that was also used to pick up the hBN. This polymer stamp was prepared on a PDMS handle as described in the work just cited, and was held on a clear quartz or sapphire substrate, during both stacking and imaging. Samples prepared in air as part of this work followed the technique developed by A.L. Sharpe *et al.*, using a manually operated stacking tool [8]. Imaging was performed with the stack still on a PC polymer stamp that was used to pick up the hBN and graphene. This polymer stamp was prepared on a PDMS handle and held on a clear glass slide, both during stacking and imaging. Post-fabrication, all samples were stored in a nitrogen drybox prior to being removed for AFM measurements.

All AFM measurements shown as part of this work were performed at Stanford university in a shared facility instrument at room temperature, in air, without any humidity or temperature control beyond the room's air-handling, on a Bruker Dimension Icon AFM equipped with NanoScope V electronics and software version 9.40 (March 2019). As a confirmation, a few test measurements were also performed outside of the facility on a Bruker Dimension Icon AFM with NanoScope 6 electronics. No modifications were made to the hardware or the software of any of the instruments to perform these measurements. A DTRCH-AM probe holder (also used for PF-TUNA or TR-TUNA), with the tip-bias wire disconnected, was used to hold AFM tips. Various AFM tips were used to measure moiré superlattices and atomic lattices. Adama Innovations AD-2.8-AS & AD-2.8-SS, Oxford Instruments Asytec.02-R2 and Mikro-Masch HQ:NSC18/Pt all showed good results. AFM images were analyzed in Gwyddion. A Standard Operating Procedure (SOP) for Torsional Force Microscopy, to aid in the reproduction of these results, is provided in supplementary materials.

Acknowledgments

We thank Peter De Wolf, Ravi Chandra Chintala, Senli Guo, Shuiqing Hu, Marcin Walkiewicz, James R. Williams, Sultan Malik, Benjamin E. Feldman, Benjamin A. Foutty, Carlos R. Kometter, Lukas Michalek, Abhay N. Pasupathy, Cory R. Dean, Mäelle Kapfer, Valerie Hsieh, Roman Gorbachev and Sung Park for fruitful discussions.

Funding

Sample preparation, measurements, and analysis were supported by the US Department of Energy, Office of Science, Basic Energy Sciences, Materials Sciences and Engineering Division, under Contract DE-AC02-76SF00515. Development of tools for robotic stacking of 2D materials were supported by SLAC National Accelerator Laboratory under the Q-BALMS Laboratory Directed Research and Development funds. All AFM imaging as part of this work was performed at the Stanford Nano Shared Facilities (SNSF), and stamps for stacking were prepared in Stanford Nanofabrication Facility (SNF), both of which are supported by the National Science Foundation under award ECCS-2026822. M.P. acknowledges partial support from a Stanford Q-FARM Bloch Postdoctoral Fellowship. D.G.-G. acknowledges support for supplies from the Ross M. Brown Family Foundation and from the Gordon and Betty Moore Foundation's EPiQS Initiative through grant GBMF9460. The EPiQS initiative also supported a symposium of early career researchers which enabled feedback from the community on this work during its development. Sandia National Laboratories is a multimission laboratory managed and operated by National Technology and Engineering Solutions of Sandia, LLC., a wholly owned

subsidiary of Honeywell International, Inc., for the U.S. Department of Energy's National Nuclear Security Administration under contract DE-NA-0003525. M.H. acknowledges partial support from the National Security Agency through the Graduate Fellowship in STEM Diversity program. K.W. and T.T. acknowledge support from the JSPS KAKENHI (Grant Numbers 21H05233 and 23H02052) and World Premier International Research Center Initiative (WPI), MEXT, Japan.

Data Availability

All data, including raw AFM images, acquired from samples presented in this work are available at the Stanford Digital Repository [42].

Duration and Volume of Study

A protocol that yielded the moiré superlattices imaged in this work was first developed in October 2022. Between November 2022 and June 2023, at least 33 regions on 32 unique samples were studied, of which 31 regions yielded at least one moiré (a success rate of 94%). 10 of these regions showed signs of two moirés, though a second moiré was not searched for and analyzed on all samples. Starting at the end of March 2023, torsional piezos were directly driven, as opposed to being indirectly driven by crosstalk. Between April and June 2023 atomic lattices of hBN and graphene were searched for in at least 8 regions of 6 unique samples, each of which yielded a discernible atomic lattice.

Competing Interests

M.A.K. currently serves as a member of the Department of Energy Basic Energy Sciences Advisory Committee. Basic Energy Sciences provided funding for this work. M.A.K. also served as an independent director on the board of Bruker Corporation until May 2023. B.P. is a senior applications scientist at Bruker Nano Surfaces. All data shown were taken on a Bruker Dimension Icon AFM at Stanford University.

Author Contributions

M.P., G.Z.J., S.J.T. and J.F., with input from C.J.N., performed the initial work on AFM imaging. M.P. identified the importance of controlling the loading force and of explicitly driving the torsional resonance in open loop. B.P. identified that instrument crosstalk was the source of torsional drive during piezoresponse force microscopy (PFM) measurements, and provided supporting evidence for this. M.P. developed the protocols for imaging both the VdW moirés and the VdW atomic lattices shown in this work. M.P. and S.J.T. imaged all samples using the protocols developed. S.J.T. led sample preparation in vacuum with the help of M.P., N.J.B. and M.H., while A.L.S., R.V.K. and S.S.K. worked on sample preparation in air. K.W. and T.T. prepared the hBN crystals from which flakes were exfoliated for use in all samples. M.A.K., A.J.M. and D.G.-G. supervised the

project. M.P. wrote the manuscript with input from all authors.

* mihirpen [at] stanford [dot] edu

† goldhaber-gordon [at] stanford [dot] edu

- [1] E. Suárez Morell, J. D. Correa, P. Vargas, M. Pacheco, and Z. Barticevic, Phys. Rev. B **82**, 121407 (2010).
- [2] S. Shallcross, S. Sharma, and O. A. Pankratov, Phys. Rev. Lett. **101**, 056803 (2008).
- [3] G. Trambly de Laissardière, D. Mayou, and L. Magaud, Nano Lett. **10**, 804 (2010).
- [4] R. Bistritzer and A. H. MacDonald, Phys. Rev. B **81**, 245412 (2010).
- [5] R. Bistritzer and A. H. MacDonald, Proceedings of the National Academy of Sciences **108**, 12233 (2011).
- [6] Y. Cao, V. Fatemi, S. Fang, K. Watanabe, T. Taniguchi, E. Kaxiras, and P. Jarillo-Herrero, Nature **556**, 43 (2018).
- [7] Y. Cao, V. Fatemi, A. Demir, S. Fang, S. L. Tomarken, J. Y. Luo, J. D. Sanchez-Yamagishi, K. Watanabe, T. Taniguchi, E. Kaxiras, R. C. Ashoori, and P. Jarillo-Herrero, Nature **556**, 80 (2018).
- [8] A. L. Sharpe, E. J. Fox, A. W. Barnard, J. Finney, K. Watanabe, T. Taniguchi, M. A. Kastner, and D. Goldhaber-Gordon, Science **365**, 605 (2019).
- [9] M. Serlin, C. L. Tschirhart, H. Polshyn, Y. Zhang, J. Zhu, K. Watanabe, T. Taniguchi, L. Balents, and A. F. Young, Science **367**, 900 (2020).
- [10] K. Yasuda, X. Wang, K. Watanabe, T. Taniguchi, and P. Jarillo-Herrero, Science **372**, 1458 (2021).
- [11] Y. Cao, D. Chowdhury, D. Rodan-Legrain, O. Rubies-Bigorda, K. Watanabe, T. Taniguchi, T. Senthil, and P. Jarillo-Herrero, Phys. Rev. Lett. **124**, 076801 (2020).
- [12] C. Wei and T. A. Sedrakyan, Phys. Rev. B **108**, 064202 (2023).
- [13] J. Shi, J. Zhu, and A. H. MacDonald, Phys. Rev. B **103**, 075122 (2021).
- [14] J. Finney, A. L. Sharpe, E. J. Fox, C. L. Hsueh, D. E. Parker, M. Yankowitz, S. Chen, K. Watanabe, T. Taniguchi, C. R. Dean, A. Vishwanath, M. A. Kastner, and D. Goldhaber-Gordon, Proceedings of the National Academy of Sciences **119**, e2118482119 (2022).
- [15] X. Wang, J. Finney, A. L. Sharpe, L. K. Rodenbach, C. L. Hsueh, K. Watanabe, T. Taniguchi, M. A. Kastner, O. Vafek, and D. Goldhaber-Gordon, Unusual magneto-transport in twisted bilayer graphene from strain-induced open Fermi surfaces (2022), arXiv:2209.08204.
- [16] C. N. Lau, M. W. Bockrath, K. F. Mak, and F. Zhang, Nature **602**, 41 (2022).
- [17] L. J. McGilly, A. Kerelsky, N. R. Finney, K. Shapovalov, E.-M. Shih, A. Ghiotto, Y. Zeng, S. L. Moore, W. Wu, Y. Bai, K. Watanabe, T. Taniguchi, M. Stengel, L. Zhou, J. Hone, X. Zhu, D. N. Basov, C. Dean, C. E. Dreyer, and A. N. Pasupathy, Nat. Nanotechnol. **15**, 580 (2020).
- [18] S. A. Sumaiya, J. Liu, and M. Z. Baykara, ACS Nano **16**, 20086 (2022).
- [19] S. Chiodini, J. Kerfoot, G. Venturi, S. Mignuzzi, E. M. Alexeev, B. Teixeira Rosa, S. Tongay, T. Taniguchi, K. Watanabe, A. C. Ferrari, and A. Ambrosio, ACS Nano **16**, 7589 (2022).

- [20] D. A. A. Ohlberg, A. C. Gadelha, D. Tamia, E. G. S. Neto, D. A. Miranda, J. S. Lemos, F. C. Santana, L. C. Campos, J. C. Ramírez, C. G. d. Rego, A. Jorio, and G. Medeiros-Ribeiro, in *Low-Dimensional Materials and Devices 2020*, Vol. 11465 (SPIE, 2020) pp. 31–37.
- [21] D. A. A. Ohlberg, D. Tami, A. C. Gadelha, E. G. S. Neto, F. C. Santana, D. Miranda, W. Avelino, K. Watanabe, T. Taniguchi, L. C. Campos, J. C. Ramirez, C. G. do Rego, A. Jorio, and G. Medeiros-Ribeiro, *Nat. Comm.* **12**, 2980 (2021).
- [22] S. Zhang, Q. Yao, L. Chen, C. Jiang, T. Ma, H. Wang, X.-Q. Feng, and Q. Li, *Phys. Rev. Lett.* **128**, 226101 (2022).
- [23] M. Kapfer, B. S. Jessen, M. E. Eisele, M. Fu, D. R. Danielsen, T. P. Darlington, S. L. Moore, N. R. Finney, A. Marchese, V. Hsieh, P. Majchrzak, Z. Jiang, D. Biswas, P. Dudin, J. Avila, K. Watanabe, T. Taniguchi, S. Ulstrup, P. Bøggild, P. J. Schuck, D. N. Basov, J. Hone, and C. R. Dean, Programming moiré patterns in 2D materials by bending (2022), arXiv:2209.10696 [cond-mat].
- [24] A. J. Marsden, M. Phillips, and N. R. Wilson, *Nanotechnology* **24**, 255704 (2013).
- [25] V. V. Korolkov, S. A. Svatek, A. Summerfield, J. Kerfoot, L. Yang, T. Taniguchi, K. Watanabe, N. R. Champness, N. A. Besley, and P. H. Beton, *ACS Nano* **9**, 10347 (2015).
- [26] S. L. Moore, C. J. Ciccarino, D. Halbertal, L. J. McGilly, N. R. Finney, K. Yao, Y. Shao, G. Ni, A. Sternbach, E. J. Telford, B. S. Kim, S. E. Rossi, K. Watanabe, T. Taniguchi, A. N. Pasupathy, C. R. Dean, J. Hone, P. J. Schuck, P. Narang, and D. N. Basov, *Nat. Comm.* **12**, 5741 (2021).
- [27] Y. Bai, L. Zhou, J. Wang, W. Wu, L. J. McGilly, D. Halbertal, C. F. B. Lo, F. Liu, J. Ardelean, P. Rivera, N. R. Finney, X.-C. Yang, D. N. Basov, W. Yao, X. Xu, J. Hone, A. N. Pasupathy, and X.-Y. Zhu, *Nat. Mater.* **19**, 1068 (2020).
- [28] L. Huang and C. Su, *Ultramicroscopy* **100**, 277 (2004).
- [29] C. Su, L. Huang, C. B. Prater, and B. Bhushan, in *Applied Scanning Probe Methods V: Scanning Probe Microscopy Techniques*, NanoScience and Technology, edited by B. Bhushan, S. Kawata, and H. Fuchs (Springer, Berlin, Heidelberg, 2007) pp. 113–148.
- [30] Q. Li, K.-S. Kim, and A. Rydberg, *Rev. Sci. Instrum.* **77**, 065105 (2006).
- [31] Bruker Corp. TR mode Support Note 416 (Rev. I) (2011).
- [32] A. Yurtsever, A. M. Gigler, and R. W. Stark, *J. Phys.: Conf. Ser.* **100**, 052033 (2008).
- [33] F. J. Giessibl, *Materials Today* **8**, 32 (2005).
- [34] S. Carr, D. Massatt, S. B. Torrisi, P. Cazeaux, M. Luskin, and E. Kaxiras, *Phys. Rev. B* **98**, 224102 (2018).
- [35] K. Zhang and E. B. Tadmor, *Journal of the Mechanics and Physics of Solids* **112**, 225 (2018).
- [36] M. M. v. Wijk, A. Schuring, M. I. Katsnelson, and A. Fasolino, *2D Mater.* **2**, 034010 (2015).
- [37] H. Yoo, R. Engelke, S. Carr, S. Fang, K. Zhang, P. Cazeaux, S. H. Sung, R. Hovden, A. W. Tsien, T. Taniguchi, K. Watanabe, G.-C. Yi, M. Kim, M. Luskin, E. B. Tadmor, E. Kaxiras, and P. Kim, *Nat. Mater.* **18**, 448 (2019).
- [38] R. Engelke, H. Yoo, S. Carr, S. H. Sung, K. Zhang, A. M. Valdivia, E. Tadmor, R. Hovden, E. Kaxiras, and P. Kim, *Microscopy and Microanalysis* **26**, 854 (2020).
- [39] Y. Song, X. Gao, A. Hinaut, S. Scherb, S. Huang, T. Glatzel, O. Hod, M. Urbakh, and E. Meyer, *Nano Lett.* **22**, 9529 (2022).
- [40] K. Walter, J. Bourquin, A. Amiri, N. Scheer, M. Dehnert, A. L. Eichhorn, and C. Dietz, *Soft Matter* **19**, 4772 (2023).
- [41] A. J. Mannix, A. Ye, S. H. Sung, A. Ray, F. Mujid, C. Park, M. Lee, J.-H. Kang, R. Shreiner, A. A. High, D. A. Muller, R. Hovden, and J. Park, *Nat. Nanotechnol.* **17**, 361 (2022).
- [42] M. Pendharkar, S. J. Tran, G. Zaborski Jr., J. Finney, A. L. Sharpe, R. V. Kamat, S. S. Kalantre, M. Hocking, N. J. Bittner, K. Watanabe, T. Taniguchi, B. Pittenger, C. J. Newcomb, M. A. Kastner, A. J. Mannix, and D. Goldhaber-Gordon, Data for: Torsional Force Microscopy of Van der Waals Moires and Atomic Lattices (2023), Stanford Digital Repository. <https://doi.org/10.25740/zj475qr8207>. Deposited 15 August 2023.

Supplementary Materials for
Torsional Force Microscopy of Van der Waals Moirés and Atomic Lattices
(Dated: 16 August 2023)

AFM measurements:

A comparison of Torsional Resonance in TFM vs Piezoresponse Force Microscopy (PFM) Modes

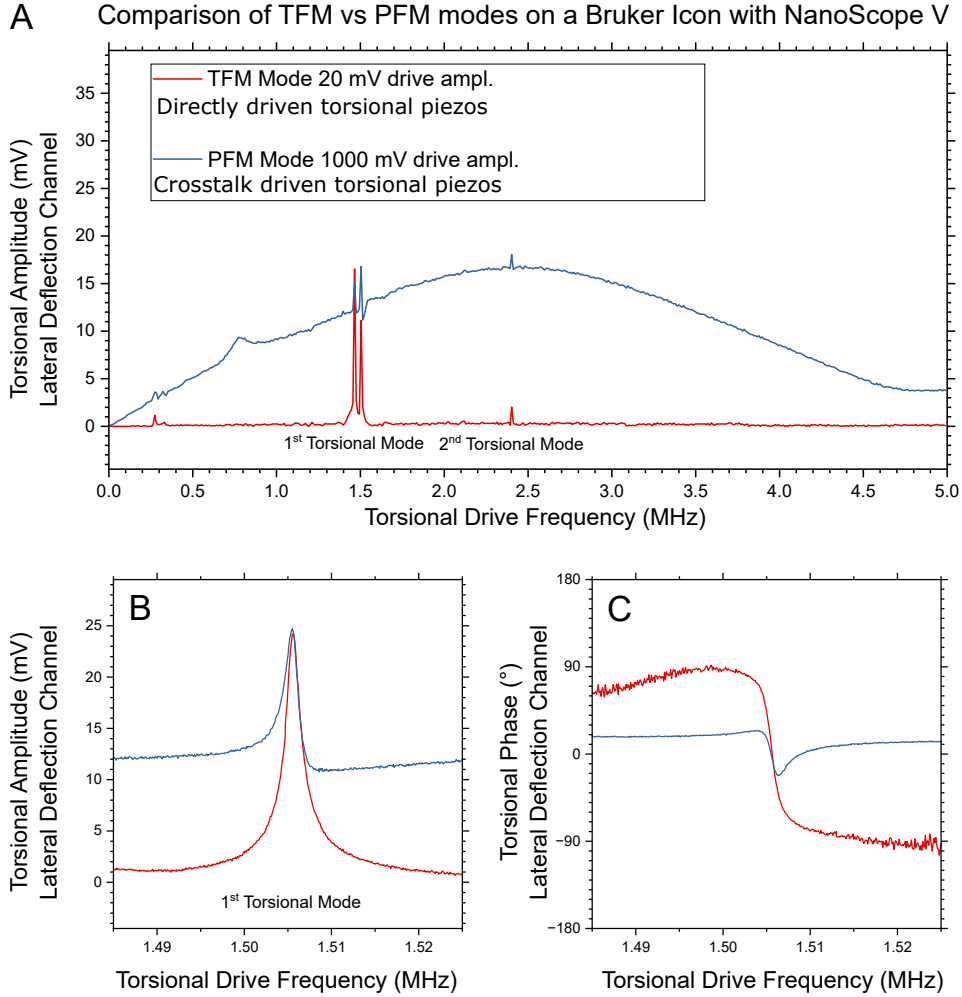


FIG. S1. **Comparison of TFM vs. PFM mode of driving the torsional piezos** The torsional resonance spectrum from near 0 to 5 MHz is shown in the blue curve in (A) and was measured in the PFM mode by parasitically driving the torsional piezos and selecting a “tip bias” of 1 V. The curve shown in red in (A) shows this resonance spectrum in the TFM mode, acquired by applying 20 mV directly to the torsional piezos (applying the excitation in PFM mode required 50x higher voltage, 1V at 1.5 MHz.) (B) and (C) show a zoom-in of the first torsional mode in amplitude and phase respectively. These comparison measurements were performed in air, without any sample in proximity of the AFM tip, on an ASYLELC.02-R2 AFM tip with a nominal first vertical bending mode at 285 kHz and a nominal spring constant of 42 N/m. For the particular AFM tip chosen here, there is a split resonance at the first torsional mode, possibly due to the properties of this particular AFM cantilever or its mechanical clamping in the probe holder. (B) and (C) zoom into one peak of that split resonance.

Prior to March 2023, our TFM measurements were performed by selecting piezoresponse force microscopy (PFM) mode in the Bruker Dimension Icon NanoScope software. However, because of the way we configured hardware electrical connections *no bias was actually applied to the tip*. Instead, through crosstalk in the electronics, torsional piezos on the probe holder were driven with amplitude of 2-2.5% of the tip bias we selected (20-25 mV of 1V). When the drive frequency was close to a MHz torsional resonance, this drive amplitude mechanically excited torsional motion in the AFM cantilever. Details: The standard DTRCH-AM probe holder we used has two special features compared to

most probe holders: torsional piezos and an electrically-insulating Macor AFM probe seat. In the software, we chose typical PFM settings: routing an AC bias voltage to the AFM tip, and electrically grounding the sample. However, the normal outcomes of these settings were defeated in hardware, as explained below. There are 4 electrical traces on this probe holder's PC board. A photo of the probe holder is shown in Fig.S7(A), though these traces are not visible. Three of the traces connect to the torsional piezos to drive the two piezos 180 degrees out of phase with each other, and the fourth trace comes to a dead end on the PCB. Software configures which signal is routed through the scan head to each trace. The prominently-visible white wire bypasses the insulating probe seat to connect electrically to the tip without routing through the scan head. We verified that disconnecting this white wire and taping it to the side of the instrument (Fig.S7(B)) had no effect on image contrast or the observed torsional resonance. Nor was the sample effectively grounded, as it was mounted on a polymer stamp atop a 0.5 mm thick quartz or sapphire substrate. The moiré image contrast we nonetheless observed when our AC drive frequency matched a torsional resonance of the cantilever was thus not from a piezoelectric response of the sample. We nonetheless refer to this as a PFM configuration because of the mode selected in software.

In PFM mode, the software-selected tip bias is routed on this probe holder to the trace that dead-ends on the PCB, while the white wire is not driven. Within the AFM scan head and the NanoScope V electronics, the wire that connects to this dead-end tip bias trace likely runs very close to the torsional piezo drive lines. Electrical crosstalk was found to carry over about 2-2.5% of the applied AC bias from the tip bias wire to the torsional piezos (2% at 1.5 MHz as shown in Fig. S1(B)), so telling the system to drive the tip electrically did not in fact bias the tip, but did parasitically drive the torsional piezos.

In a newer version of the electronics (NanoScope 6), this crosstalk was found to drop to about 1% based on a direct measurement of the voltage on the wires leading to the torsional piezos in the DTRCH-AM probe holder.

Drawbacks of performing TFM measurements in PFM mode include: 1. Crosstalk is not an intentional part of the instrument design, so its amount may vary between instruments and probe holders (even with the same model number.) 2. The crosstalk-driven resonance in PFM mode produced an exceedingly high background signal as measured in the lateral deflection channel, leading to a poor SNR (see Fig. S1(A)&(B)). 3. The PFM mode lacks some very useful software tools that are provided in the TR mode, which is intended for operating torsional piezos: a. option to balance the left and right piezos to optimize driving torsional resonances of a cantilever. b. option to check whether the torsional signal observed is due to torsional motion or due to unintentional coupling of vertical motion into the lateral deflection channel of the photodetector. For these reasons we have transitioned to enacting TFM explicitly in TR mode, instead of nominally performing PFM and relying on crosstalk to excite a torsional resonance.

AFM measurements: Additional results

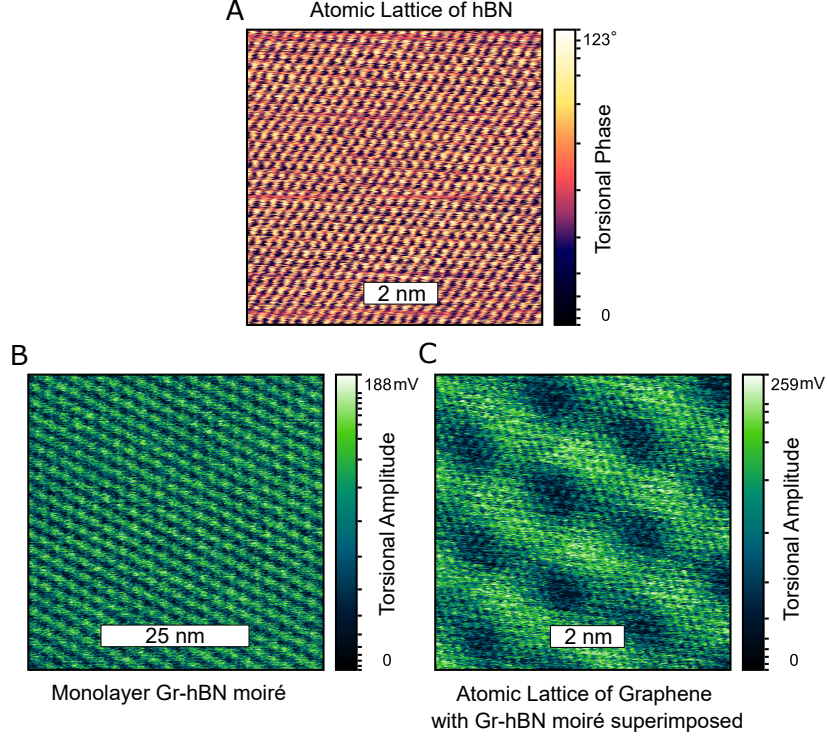


FIG. S2. Atomic Lattice of hBN & Gr and moiré of monolayer Gr-hBN Continuing from Fig. 2 of the main text, (A) shows the torsional phase corresponding to the torsional amplitude shown in Fig. 2 (A). (B) and (C) show the torsional amplitude of the torsional phase images shown in Fig. 2 (B) and (C). Images shown here and in Fig. 2 were processed using the align rows function in Gwyddion using polynomial fitting, followed by fixing zero to the bottom of the scale. The data was then plotted on an adaptive color scale to enhance lattice contrast. Imaging was performed using an Adama Innovations AD-2.8-SS AFM tip with a ratio of response to drive of 15 mV/mV when measured in air and away from the sample, at the 1.42 MHz resonance.

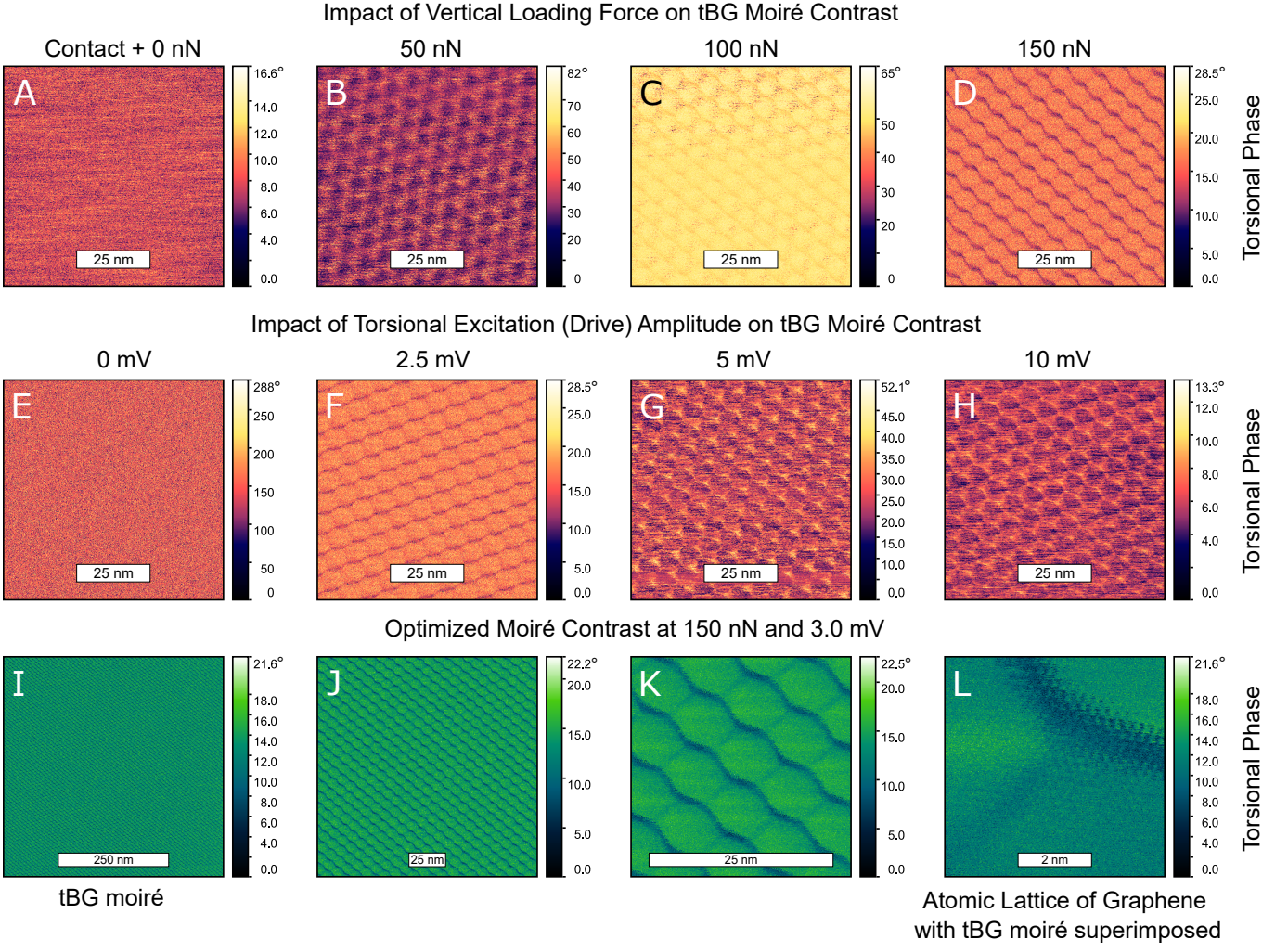


FIG. S3. Imaging moirés in tBG: Impact of Vertical Loading Force & Resonant Torsional Excitation Amplitude on Moiré Contrast Continuing from Fig. 3 of the main text, (A-L) are torsional phase counterparts of the torsional amplitude images shown in Fig. 3 of the main text. Images shown here and in Fig. 3 were processed using the align rows function in Gwyddion using polynomial fitting, followed by fixing zero to the bottom of the scale. The data were then plotted on a linear color scale. Data scale for main text Fig. 3 panels (K-N) has been restricted uniformly to 100 mV to provide a direct perspective of how the image evolves as zoomed in at the same imaging settings. Imaging was performed using an Adama Innovations AD-2.8-SS AFM tip with a ratio of photodetector response to piezo drive of 30 mV/mV when measured in air and away from the sample, at the 1.45 MHz resonance. At the time of imaging, the sample was over 5 months old and no prior surface cleaning or treatment was performed on this sample. Typically, the sample was stored in nitrogen environment with frequent removal to air for days during AFM imaging sessions.

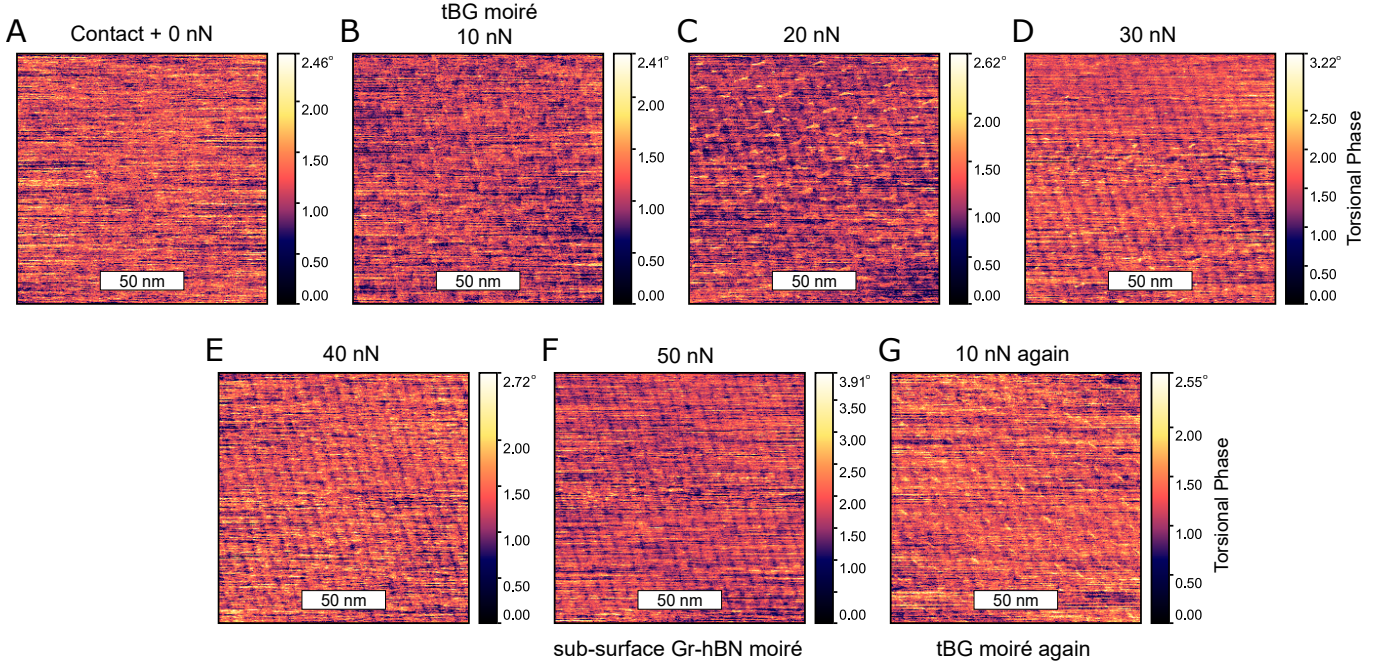


FIG. S4. Imaging a subsurface moiré Continuing from Fig. 4 of the main text, (A-G) are torsional phase counterparts of the torsional amplitude images shown in Fig. 4 of the main text. Images shown here and in Fig. 4 were processed using the align rows function in Gwyddion using polynomial fitting, followed by fixing zero to the bottom of the scale. The data were then plotted on a linear color scale. Data scale for main text Fig. 4 panels (B-H) has been restricted uniformly to 300x0.05 mV to provide a direct perspective of how the image evolves as force is stepped at the same imaging settings. Imaging was performed using an Adama Innovations AD-2.8-AS AFM tip with a ratio of response to drive of 0.125 mV/mV when measured in air and away from the sample, at the 1.32 MHz resonance. The lower ratio of response to drive is due to the image being taken with indirectly- rather than directly-driven torsional piezos.

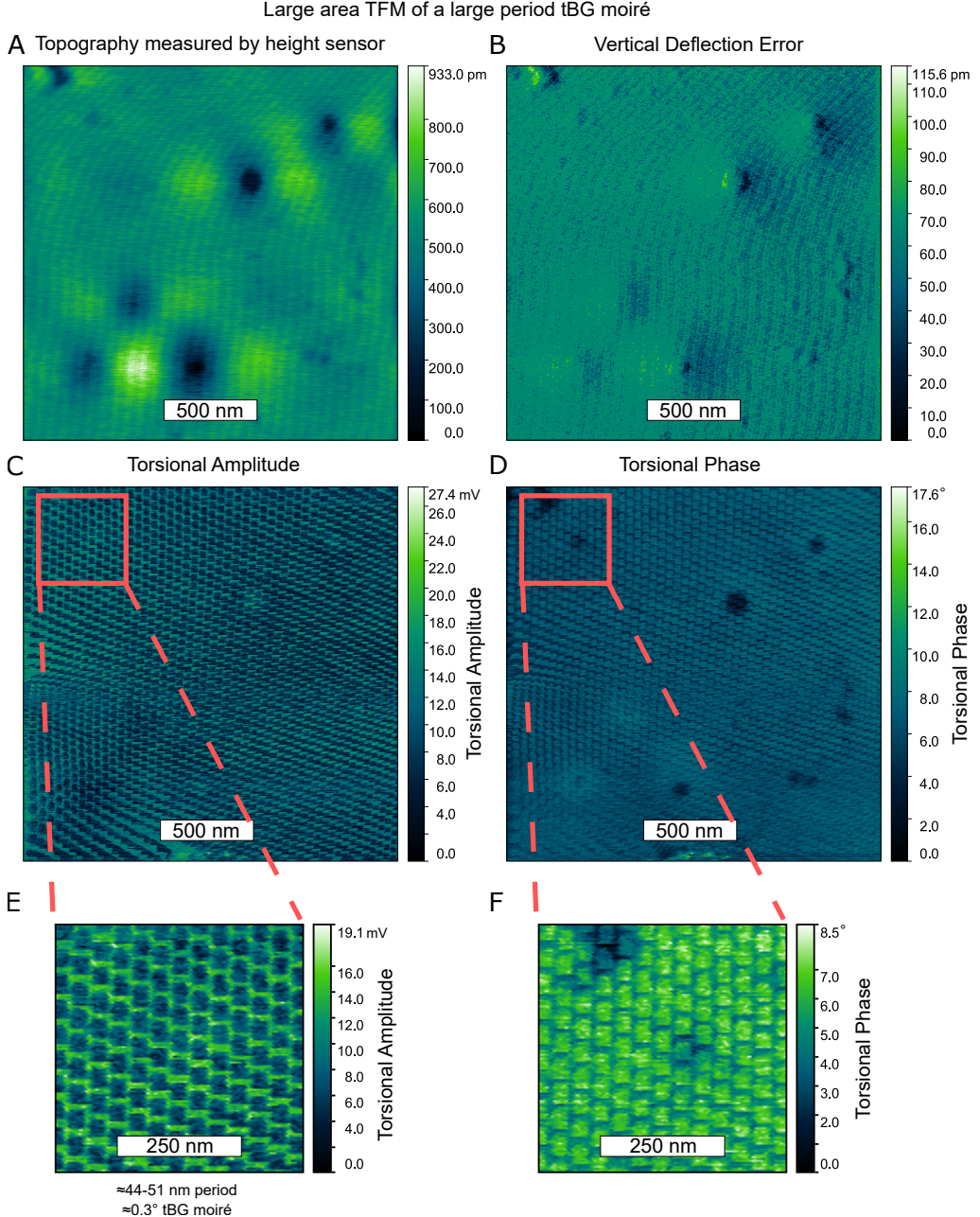


FIG. S5. Large area TFM of a large period tBG moiré superlattice TFM was tested on a tBG stack (prepared in vacuum) over a $2 \times 2 \mu\text{m}^2$ region –dimensions relevant to electronic devices. (A) shows the topography measured by a height sensor and (B) shows the vertical deflection error as compared to the deflection setpoint. The faint parallel lines in (A) and (B) were determined to be periodic instrument noise. (C) and (D) show the TFM amplitude and phase, respectively. (A-D) were acquired simultaneously as separate measurement channels of the same scan. The variation of the moiré period over the area imaged is apparent in (C) and (D). (E) and (F) are digitally zoomed-in views of (C) and (D), respectively. The moiré period in (E) varies from about 44–51 nm, corresponding to a twist angle of 0.3° in tBG. Images shown here were processed using the align rows function in Gwyddion using polynomial fitting, followed by fixing zero to the bottom of the scale. The data were then plotted on a linear color scale. The scan parameters were: Loading force of nominally 200 nN with a torsional drive amplitude of 50 mV at the 1.210 MHz torsional resonance and a line scan speed of 1.0 Hz. The scan angle was 90° and a 16x signal amplifier was enabled. Imaging was performed using an Oxford Instruments ASYLELC.02-R2 AFM tip with a ratio of response to drive of 10 mV/mV when measured in air and away from the sample.

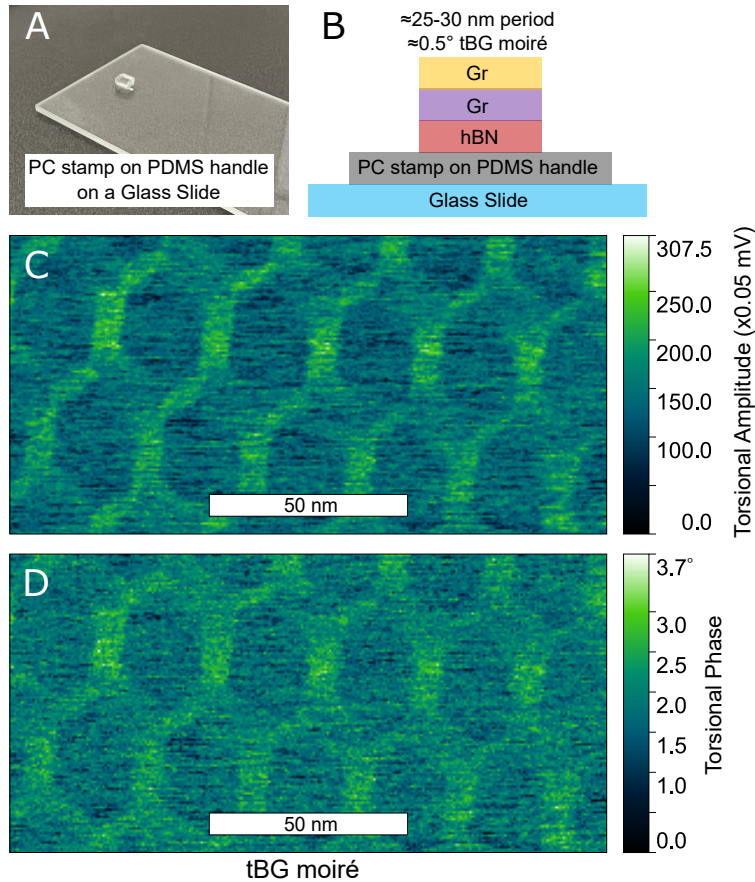


FIG. S6. TFM of tBG on a PC stamp placed on a PDMS handle on a glass slide To confirm the operation of TFM on VdW heterostructures held with other common stamp surfaces, a tBG sample prepared in air on a Poly(Bisphenol A carbonate) (PC) stamp was imaged. During both stacking and imaging, this sample was held on a PDMS handle placed on a glass slide. These results show the versatility of TFM and its use in rapid feedback on stack synthesis: PC-on-PDMS-stamps held on a glass slide are commonly used to stack multiple successive VdW layers. The moiré period is about 25-30 nm with a computed corresponding twist angle of 0.5°. This measurement was performed with indirectly driven torsional piezos. Images shown here were processed using the align rows function in Gwyddion using polynomial fitting, followed by fixing zero to the bottom of the scale. The data were then plotted on a linear color scale. The scan parameters were: Loading force of nominally 50 nN with a 1000 mV drive amplitude at the 1.294 MHz torsional resonance and a line scan speed of 0.5 Hz. The scan angle was 0° and a 16x signal amplifier was enabled. Imaging was performed using an Adama Innovations AD-2.8-AS AFM tip with a ratio of response to drive of 0.011 mV/mV when measured in air and away from the sample. For this particular sample, the moiré contrast improved as force was stepped up from “Contact + 0 nN” to 75 nN, at which point the high force led to a tear in the sample. The tear likely occurred due to a sharp AFM tip and a comparatively soft polymer structure (PC-on-PDMS as compared to our vacuum-compatible lithographically-patterned stamps.) When using a new type of stamp or AFM tip, force must be stepped up carefully and the effect on images examined. Once acceptable moiré contrast has been obtained, any further increase in force to enhance contrast must be approached with caution.

Torsional Force Microscopy: a Standard Operating Procedure (SOP) to image VdW moiré superlattices and atomic lattices

This SOP aims to provide the necessary guidance to enable the reader to replicate the results of this work performed on a Bruker Dimension Icon AFM with NanoScope V electronics at Stanford University. It has been written assuming the reader has a basic working knowledge of operating the instrument in contact and non-contact AFM modes. This SOP is merely a suggested set of steps and not a substitute for instrument manuals, or for taking care to secure the safety of the instrument, samples, and/or users. As this protocol evolves, an updated version of this SOP may be made available [42]. Additional information about setting up the instrument for torsional resonance can be found elsewhere [31].

An “ingredient list” for TFM:

1. Probe holder with torsional piezos.

- (a) An AFM probe holder with torsional piezos, to mechanically excite the torsional resonance, is required for TFM. We worked with a DTRCH-AM probe holder (see Fig. S7(A)).
- (b) Any signal preamplification box or other associated hardware is not required for TFM and does not need to be installed.

2. AFM tips.

- (a) Adama Innovations AD-2.8-AS & AD-2.8-SS, Oxford Instruments Asytec.02-R2 and Mikro-Masch HQ:NC18/Pt have been tested to work, including for atomic lattice imaging.
- (b) AFM tips resistant to wear were preferred since some experiments required application of nominal forces exceeding 100 nN.

3. Sample to be imaged.

- (a) For tBG and Gr-hBN samples, a fresh sample and a fresh AFM tip were not found to be necessary for imaging a moiré superlattice, but moiré contrast was often visibly improved with both a fresh sample and a fresh tip.
- (b) For atomic lattice measurements of hBN, samples as old as a few years and stored in air showed a discernible atomic lattice. Atomic lattices of other materials may behave differently. Fresh samples are preferred for determination of initial imaging settings.

Setting up the hardware for TFM:

1. Put tip in probe holder & install the probe holder.

- (a) The DTRCH-AM probe holder places the AFM cantilever on a Macor seat that electrically isolates the cantilever from the rest of the probe holder. The cantilever is secured by a clamp which has a white wire that provides the only electrical contact to the AFM tip (see Fig. S7(A)). This white wire is left disconnected and taped to the side of the scan head such that the tape ensures the metal end of the wire does not come in contact with the chassis of the AFM as shown in Fig. S7(B).
- (b) It may be best to center the AFM tip in the white Macor seat of the probe holder.
- (c) The screw on the clamp, holding down the AFM tip, should be reasonably tight. Over-tightening dampens the resonance. It may take a few tries with the same AFM tip and comparing torsional resonances, to fully gauge the optimal setting.
- (d) We also aimed to put the AFM tip in the center of the field of view of the camera when it was fully zoomed out (no digital zoom) and aimed to align the long axis of the cantilever parallel to the camera image frame. The incident laser was found to be most focused near the center of the field of view with significant distortions at extremities. Results may vary dramatically if the laser is not focused on the AFM tip.
- (e) An anti-static gun for the tip and the sample may be useful but was not tested.
- (f) While no drawbacks are anticipated spurious voltages on scan head may affect the electrostatic potential at the tip sample interface and worse, may change during scan affecting imaging conditions.

2. Put the sample in place & turn on the vacuum.

Note: Double-sided tape to hold the sample was not tested and may not be well suited.

Setting the NanoScope software for TFM

1. Creating a Logbook.

- (a) A table with the following columns, created in an online or offline spreadsheet, accessible post-imaging, should suffice.
- (b) This log will be called upon in the following steps as “Make a logbook entry” without further details. All applicable fields should be entered at that time and will be required for accurate estimation of force during imaging,

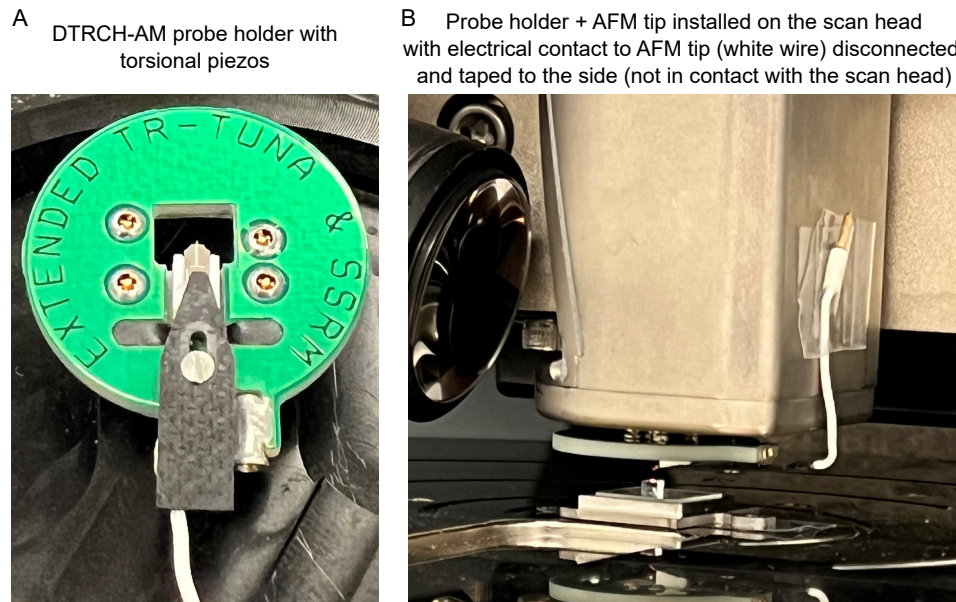


FIG. S7. Torsional probe holder (A) DTRCH-AM torsional probe holder with an AFM tip inserted. The tip is seated on an electrically insulated piece of Macor, under which the two torsional piezos are housed. A clamp (in black) holds down the AFM tip and is also the only electrical contact to the AFM tip with a white wire connected to it. (B) Probe holder installed on the scan head, with the white wire taped to the side of the scan head to ensure it doesn't make contact with the chassis.

though it would be best to enter all possible values as often as one can.

- (c) The log should have the following eight columns:
 - i. Time
 - ii. Signal Sum (volts) – only an approximate value will be available after imaging begins.
 - iii. Vertical Deflection (volts) – here, this represents the free vertical deflection of the cantilever in air, far from the sample. The value displayed in the software after imaging begins will not represent this free deflection and hence the vertical deflection column should be left blank after imaging begins. The feedback loop will try to ensure the vertical deflection is the same as the setpoint.
 - iv. Horizontal Deflection (volts) – here, this represents the free horizontal deflection. Since there is no feedback loop that relies on this value, a drift of this deflection should not have immediate consequences to image quality. Yet, for developing an understanding of instrument drift, logging this deflection is necessary.
 - v. Flying Condition (volts) – this represents the deflection setpoint, in volts, at which the tip retracts from the surface when imaging, i.e. “flies away”. This will be a

proxy for vertical deflection during imaging albeit it may be affected by electrostatics due to the proximity of the sample surface. The tip can be considered withdrawn when the “z-piezo” indicator in the software turns red and shows the tip has moved all the way up. Recording this flying condition would require pausing imaging and reducing the voltage setpoint every 30-60 minutes to determine how much the free vertical deflection has truly drifted by.

- vi. Last Point of Contact (volts) – this represents the deflection setpoint at which the tip is still in contact but any further reduction of setpoint makes the tip retract (fly away) from the surface. This will be logged in conjunction with the flying condition above. This deflection setpoint will also be referred to as “Contact + 0 nN” as it is the minimum force required to remain in contact with the sample in addition to any force that may be required to remain in contact.
- vii. Snapback (volts) – this represents the deflection setpoint at which the tip returns to making stable contact with the surface (the piezo indicator should be roughly in the middle of its range and green) after having previously retracted from the surface. Due to attractive/repulsive interac-

tions between the tip and the sample, this deflection setpoint will differ from the last point of contact, but not by more 10s of nN.

- viii. Notes – enter comments like “Laser aligned”, “enclosure closed”, “about to click engage”, “approached on hBN”, “on tBG”, “retracted”, etc.

2. Starting “Torsional Resonance” experiment.

- (a) This experiment will now configure the electronics to directly drive the torsional piezos.
- (b) When setting up for the first time, select “Tapping Mode” followed by “Tapping Mode in Air”, then “Torsional Resonance (TR-Mode)” and click “Continue”.

Note: Due to the number of settings that have to be changed, it is best to save the experiment once it has been correctly configured and then re-open the saved experiment every time afterwards. There is a step below to save the experiment for opening in future runs.

- (c) When opening a saved experiment:
 - i. Select Cancel on the experiment selection window that pops up.
 - ii. From the “Experiment” menu in the row up top, select “Open experiment” and open the saved TFM experiment.
 - iii. The steps below on configuring the experiment in “Scan window” and configuring the “Engage settings” can now be skipped as they will be recalled with the saved experiment. Jump to “Align the laser on the cantilever”.

3. Scan window.

- (a) With the experiment now open, it will begin with the “Scan” option selected from the column on the left where “Scan”, “Engage” and “Withdraw” are show. If not, select “Scan” from that column.
- (b) Set the file name for scans and select the user data folder.
- (c) In the list of scan settings, right click on white space and select “Show all” to show all the previously hidden scan settings.
 - i. With all scan settings visible, go to “Other”, “Microscope Mode” and select “Dynamic Friction”. This configures the instrument to operate in a contact AFM like mode with a feedback loop maintaining a constant vertical deflection setpoint,

irrespective of the torsional resonance settings.

- ii. Next, go to “Scan”, “XY Closed Loop” and set it to “Off”. This will make all motions of the piezos inaccurate but is necessary for fast line scan speeds. Instead, the X-Y sensor data can be recorded as separate channels to correct for the inaccuracy, as much as possible, in postprocessing.
- iii. Ensure that under “Torsion”, “TR Mode” is be set to “Enabled”.
- iv. Ensure full Z range of the fine piezos is shown in “Limits”, for “Z limit” and “Z range”. This should be about 13-14 μm . If not, entering 15 (out of range) should automatically ensure these values are set to their maximum.
- v. Ensure “Amplitude Range” and “TR Amplitude Range” are both “4000 mV”.
- (d) Next, the “Generic Sweep” button should be visible in the left most column. If it is not visible, from the options on the top of the window, select “Experiment” and configure the experiment environment to make “Generic Sweep” appear. Generic sweep will be used extensively during imaging to track the torsional resonance.

4. Engage Settings.

- (a) From the top of the window, select “Microscope” and select “Engage Settings”.
- (b) In the “Engage Parameters” window that pops up, right click in the white space and select “Show All”.
- (c) In “Stage Engage” options, for “SPM Engage Step”, type in 0.02 μm . This will automatically set the minimum approach step to a value of about 0.035 μm (35 nm per step; the value of 20 nm previously entered was out of range and hence the minimum value was automatically selected). This can be increased to 100 nm if the approach is too slow.
- (d) With “Sample clearance” being set to 1000 μm and “SPM safety” set to 100 μm , it takes about 1-2 minutes to make contact with the surface with 35 nm per step.
- (e) Ensure in “Smart Engage” the “Engage Mode” is set to “Standard”.
- (f) Do not change any other parameters. Incorrect parameters or a step size of microns in TR mode can lead to sharp tips damaging the surface of soft polymer stamps and also becoming blunt in the process.

5. Align the laser on the cantilever

- (a) Select “Setup”, in the left column, to manually align the laser on the cantilever.

Note: Since the amplitude of torsional motion is the highest near the free end of the cantilever (on the same end as the AFM tip), the laser should be positioned as close to the free end, while still ensuring a high value of signal sum. Values typically in excess of 5 volts were common for Au coated diamond probes and in excess of 4 volts for Ti/Ir coated probes.

Note: A focused laser spot may be $40 \times 25 \mu\text{m}$ with additional lower intensity spots on either side of this ellipse.

- (b) Select the correct AFM tip from the list of AFM tips.

- i. Note the deflection sensitivity in nm/V and the nominal spring constant of the AFM tip in N/m or nN/nm
- ii. Thermal tune or other techniques can be used to estimate the above two parameters more accurately, if needed, but were not available in our version of the software within the torsional resonance mode.
- iii. Estimate the deflection in mV, per nN of force applied. It is the inverse of the value obtained by multiplying the deflection sensitivity and spring constant ($\text{nm/V} \times \text{nN/nm} = \text{nN/V}$). For example, for a deflection sensitivity of 60 nm/V and a spring constant of 2.8 nN/nm, this comes out to about 6 mV/nN. This means that if the force has to be increased by 100 nN, the deflection setpoint must be increased (made more positive) by 600 mV.

- (c) Move to the alignment station.
- (d) Align the laser on the AFM tip to 0 volts (0,0) on both vertical and horizontal deflection indicators.

- (e) Make a logbook entry.

Note: Do not move the laser or mirror deflection knobs once the laser is set as close to 0,0 as possible. The laser will heat up the cantilever and the vertical deflection value will start to drift (almost immediately) towards a more negative or positive value. This drift is expected and should reach a steady state in about 30 to 120 minutes, though the drift not reaching a steady state does not hinder measurements (logbook entries just need to be made more often, to accurately estimate the force).

- (f) Return from alignment station

- (g) Make a logbook entry.

Note: Now, it is important not to touch any of the knobs on the scan head, even if the signal keeps deviating away from 0,0 volts – we should be able to correct for the drift.

6. Cantilever tune

- (a) With the laser aligned, click on “Cantilever Tune”.
- (b) In the tuning window that pops up, we won’t be making use of the “Auto Tune” function.
- (c) Right click on the white space in the settings column on the right and select “Show all”.
- (d) The goal here is to search for a torsional resonance, and confirm that it is not a spurious vertical resonance coupling into the lateral channel (see the section on Coupling Check below) and then determine the ratio of response to drive amplitude.
- (e) Copy all settings as shown in Fig. S8.
- (f) Set the two plots to auto scale by right clicking in the plot area and selecting “Auto scale”.
- (g) Search for resonances, with a 1500 kHz center and a 3000 kHz width. At least two should show up, with a drive of 10 mV and 0.211 kHz bandwidth on the lock-in amplifier. If needed, save all spectra by clicking “Save Curve”.
- (h) The resonance spectra will look similar to plots shown in Fig. 1(D) & (E) of the main text and Fig. S1
- (i) The resonance with the tallest peak can then be selected and a frequency window of about 500 kHz can set with the resonance at the center.
- (j) Coupling check:
 - i. Next, set “Coupling check” to “On”.
 - ii. This mode replaces the displayed lateral amplitude with vertical amplitude, while continuing to drive the torsional resonance.
 - iii. A purely torsional or lateral signal should not appear on the vertical deflection channel, with coupling check turned on.
 - iv. If the resonance peak chosen appeared due to crosstalk from a vertical resonance, the previously observed peak or a shoulder of it (from the lateral channel) should become stronger. In such a case, this peak should not be chosen for imaging. If many such coupled peaks appear often, a different probe holder or different mounting of AFM tips must be tested.

- v. Next, set turn off coupling check, as imaging will be performed with coupling check turned off.

(k) Balance tune.

- Next, reduce the frequency window to between 50 kHz to 5 kHz with the resonance at the center.
- Click “More” at the bottom of the screen and select “Balance Tune”.
- The instrument will automatically select the maxima of resonance after this.
- Ideally, 0V and 10V refer to driving either the left or the right piezos with 5V on balance indicating both the piezos are being driven equally. An ideal placement of an AFM tip should lead to values around 5V

Torsional Resonance - Cantilever Tune Settings

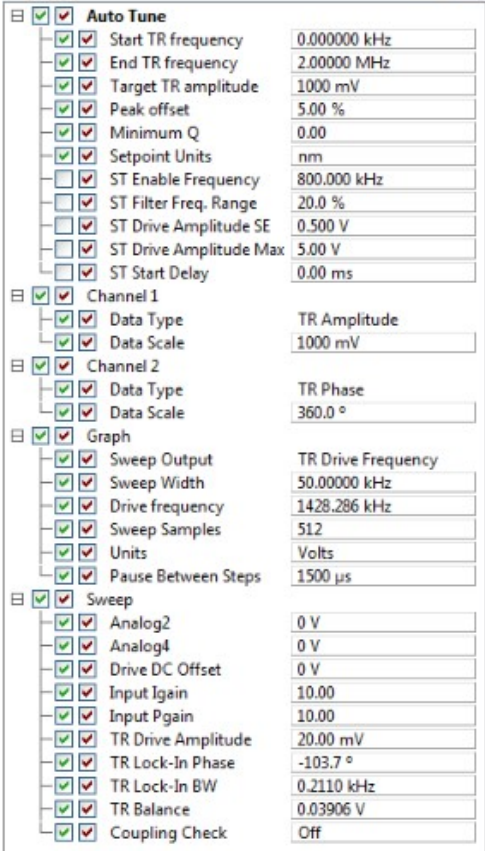


FIG. S8. **Cantilever tune settings** The cantilever tune settings are shown here as an example and may vary between cantilevers, probe holders and AFMs. Manual tune was used to first identify resonances in the torsional frequency spectrum and then using coupling check, were confirmed not to originate from crosstalk with vertical bending modes. Then with a finer frequency sweep centered at the resonance, the piezo balance was tuned and torsional drive amplitude for initial approach was set.

on balance tune showing a maxima in resonance.

Note: Software bug: As of this writing, a bug in the software limits the usability of this feature and a local maxima is observed at either 0 or 10V of balance tune, which is selected.

v. Zero the phase by clicking “Zero phase”.

- In “Sweep”, set “TR drive amplitude” to 2 mV. A clear resonance at low drive voltages has been found to aid in imaging atomic lattices.

(m) Exit cantilever tune.

Note: Since this is the first instance after aligning the laser where significant time has elapsed. The vertical deflection value should have drifted from the previously set 0V to a few hundred millivolts. The sign of this drift and the magnitude are both indicators of the drift that would have to be corrected when imaging.

- Make a logbook entry.

7. Navigate to sample.

- Find and focus on the sample, but aim to land on a region that is not critical as there is always a risk of the AFM tip damaging the surface if approach parameters are not chosen correctly. For a tBG/hBN open face structure, making initial contact on hBN is better than making initial contact on tBG.

- Make a logbook entry.

8. Check parameters:

- From the settings shown in Fig. S9, copy all the settings from the “Scan” and “Feedback” categories.
- In “Torsion”, the value for “TR Deflection Setpoint” will determine the force after contact and during imaging. It should be set to about 50 nN with respect to the “current” vertical deflection value. For example, if the vertical deflection is -400 mV (negative) and the AFM tip applies 1 nN for every 6 mV of signal, applying 50 nN (+300 mV) requires that -100 mV be entered in the TR Deflection Setpoint. Forces less than 50 nN may also work depending on the AFM tips used.

- Make a logbook entry.

- All the other settings in the “Torsion” category should have been carried over from cantilever tune, though the lock-in amplifier band width can be increased to 1 kHz to enable fast imaging initially.

- (e) In the “Other” category, ensure the tip bias control and sample bias control are both set to “Ground”.

Check Parameters - Engage Ready Settings

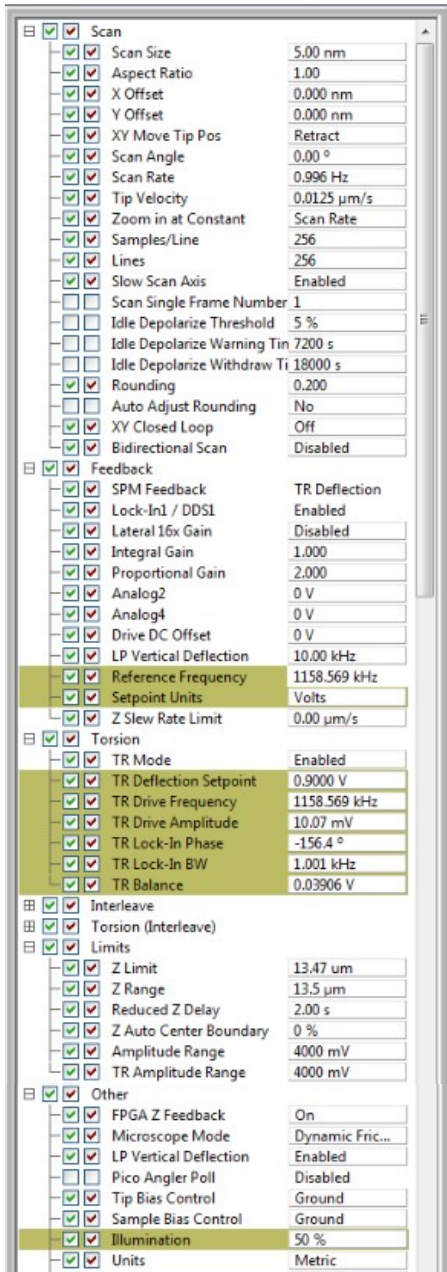


FIG. S9. Check parameters - Engage Ready Settings
An example of the check parameters window is shown, immediately prior to engaging with the sample. A few key checks include confirming the “current” vertical deflection value and appropriately choosing the “TR Deflection Setpoint”, in volts, to make contact at about a nominal force of 50 nN.

9. Save the experiment and these workspace settings (to save time in future runs):

- (a) From check parameters window, go back to

navigate and then to setup, to see the cantilever again.

- (b) Make a logbook entry.
- (c) Then from the Experiment menu at the top of the screen, save the experiment. This should save two files: experimentname.wks and experimentname.bag and enable recalling all the settings configured until this point the next time the instrument is turned on and this experiment started. Remember the location this experiment is saved to start from here.
- (d) Next, click on navigate to confirm if the region of interest is where to approach on the sample, and then click on check parameters to ensure a roughly 50 nN force is still what has been set by the TR Deflection Setpoint and the current value of vertical deflection.

10. Engage.

- (a) With the chosen force setpoint, engage the AFM tip with the sample.

Note: It should take about a minute or two to engage. If the AFM tip is about 15 μm tall, the contact should be made with the sample at about 85 μm indicated by the current position indicator at the bottom of the screen.

Note: Keep an eye on the vertical deflection setpoint during engage. If it shifts dramatically as the tip nears the sample but while its still not in contact, it indicates an electrostatic repulsion or attraction. Approach settings would then have to be tweaked accordingly.

Imaging with TFM:

1. Setting up for imaging.

- (a) After a successful contact has been made, the instrument will start scanning the small scan region chosen entered previously.
- (b) The channels to be imaged would be “Height Sensor”, “TR Deflection Error”, “TR Amplitude”, “TR Phase”, “X Sensor”, “Y Sensor”. All channels should have no “OL” or Off-Line plane fitting, and the “RT” or Real-Time plane fitting set to “Line”. It may be beneficial to record all of the above channels for either trace or retrace while the remaining two channels can be TR Amplitude and TR Phase for the opposite scan direction.
- (c) Record movie continuously or “forced” should also be enabled so that the data can now be saved.

- (d) To scan larger areas, increasing the P & I settings may be required, depending upon the undulations in the sample. Values of the order of 4 (I) and 8 (P) should enable imaging over tens of microns of scan areas with 100s of nm undulation, but these may vary from instrument to instrument.
- (e) Next, we increase the scan area to find the region of interest (R.O.I.). This initial region of interest can be something close to the most critical R.O.I. as there is another round of optimization of force and drive frequency before we can image the most critical R.O.I.

Note: From the main text, “Typical line scan speeds (each line consisting of both trace and retrace) ranged from 2 Hz over microns, to 4 Hz over hundreds of nanometers and 30 Hz over tens of nanometers. At these speeds, the lock-in amplifier input bandwidth was typically set between the lower end of 0.211 kHz (limited by electronics) to 10 kHz, with increasing bandwidth at increasing speeds, to avoid digitization.”. Adjust the scan speed and bandwidth accordingly.

- (f) Once the R.O.I. has been identified, reduce the scan area down to about 100 nm.
- (g) Then reduce the Z limit to about 4 microns. This should limit the Z range also. This option may not be available in newer versions of software and hardware.
- (h) Next, determine “Contact + 0 nN”:

- i. Reduce the “TR Deflection Setpoint”, by 10 nN approximately. i.e. if the setpoint where the sample was successfully approached and the scanning is stable was -0.1 V, make it -0.15V or -0.2V. Observe the voltage on the Z piezo.
- ii. At one such value the voltage on the Z piezo will become very negative, with the bar turning from green to yellow then red, indicating the piezo has retracted and is not tracking the surface anymore.
- iii. The goal is to determine within 10 mV the deflection setpoint at which the piezo retracts. For this, increase the setpoint again by about 0.2V to put the AFM tip back in contact and repeat the process, but with more finer steps as the “flying condition” is nearing.
- iv. Make a logbook entry of the flying condition and the last point of contact.
- v. Then slowly increase the force in 10 mV steps to put the tip firmly back in contact, at which point the Z piezo will re-

main centered in the green region and the Z voltage value shown next to it will not change as the setpoint is increased. When the AFM tip first snaps back in contact, the deflection setpoint can be logged under the “Snapback” column. This value is more for information and troubleshooting and would not be necessary for imaging.

- vi. Make a logbook entry.
- vii. Next, with the “Contact + 0 nN” force determined, set the value to either 10 or 20 nN, by setting the appropriate deflection setpoint.
- viii. This process of determining “Contact + 0 nN” should be repeated every 30 minutes if the vertical drift is found to be large or every 60-120 minutes if its small. After the first few hours of imaging, the instrument should reach a steady state where this drift should become negligible over hours.
- ix. In the remaining text, if determine “Contact + 0nN” is called, repeat the above sequence again.
- x. Every time an imaging surface is changed, i.e. for example going from tBG to hBN and vice versa, this process must be repeated as tip-sample interaction can dramatically alter the force applied for nominally the same values of “TR Deflection Setpoint”.
- (i) Next, determine the peak of torsional resonance:
 - i. During contact, due to interactions with the sample, the resonant frequency of the torsional resonance may have shifted (typically to more positive values).
 - ii. Open the “Generic Sweep” window by click on the button on the left.
 - iii. In the window that pops up, enter 0 nm. This will ensure the AFM tip remains in contact as the sweeps are being taken.
 - iv. The sweep window is similar to the cantilever tune window, but now with the auto tune function removed.
 - v. The goal is to plot the TR Amplitude in Channel 1 and TR Phase in Channel 2 (set both scales to auto scale) and find the torsional resonance peak.
 - vi. If a chosen peak doesn’t yield desired results, other peaks (which are confirmed to be not present in the vertical deflection channel, using coupling check) can be chosen.

- vii. After contact, the torsional resonance amplitude typical reduces from that in air, and the resonance frequency also shifts to a higher value. To find the peak, if it is not immediately apparent, increase the torsional drive amplitude to 10 or 20 mV and set the sweep width in the “Graph” category to about 100 kHz. A peak shift of about 1 kHz may not be surprising. The shifts will greater when the force is ramped up above 100 nN to search for moiré superlattices.
 - viii. Once the peak has been found, select “Center peak” to center it and “Zero phase”. If auto centering doesn’t work, use the offset and execute buttons to manually select the peak.
 - ix. Resonances with measured amplitudes between 10 to 50 mV would be sufficient for imaging though optimal conditions may vary between instruments.
 - x. The impact of lock-in bandwidth can also be tested here. With the bandwidth set to 0.211 kHz, the noise on the resonance spectrum should be negligible. As bandwidth is ramped up, noise in both amplitude and phase should increase.
 - xi. A bandwidth of 1 kHz may be best suited for initial imaging and can be optimized later.
 - xii. Every time an imaging surface is changed, for optimal imaging, for example going from tBG to hBN and vice versa, this process must be repeated as tip-sample interaction can shift the torsional resonance.
 - xiii. Return to scan window by clicking “Exit”.
- Note: Software bug: As of this writing, exiting out of the generic sweep window in the torsional resonance mode resets the lock-in amplifier bandwidth to an arbitrarily high value (between 80 to 200 kHz). This value must be immediately, manually, set to the desired values in the “Torsion” category under “TR Lock-in BW” field. This bug will reset the bandwidth almost every time the generic sweep window is opened and some parameters tweaked.

2. Imaging moiré superlattices

- (a) An example of imaging conditions for moiré superlattices is shown in Fig. S10 (A).
- (b) With the above complete, move into the R.O.I. where a moiré superlattice is expected.

- (c) With the force set to Contact + 10 nN or 20 nN, image over the region of interest and zoom into the about 100 or 200 nm square. The scan speed, points per line and lock-in bandwidth can all now be increased.
- (d) Then, lower the force to Contact + 0 nN and image the region.
- (e) Step up the force in steps of 10 nN until a moiré appears – in either amplitude or phase or both. For example, if the most recent “Last point of contact” was -0.1 V, then increase the force to -0.04V, +0.02V, +0.08V and so on. Sudden increases in force may damage both the AFM tip and sample as this is essentially a contact AFM technique.
- (f) Once the moiré contrast is optimized at a set force with a set torsional drive amplitude, open the sweep window again and tune to the peak of torsional resonance as it may have shifted with the increased force.
- (g) Then, step through torsional drive amplitudes to optimize contrast further. Starting from about 2.5 mV, increase the drive amplitude in steps of 2.5 mV and observe the changes to the moiré superlattice. A sign that the drive amplitude is too high is when sharp features of the superlattice become broadened. The lowest torsional drive that yields the desired results is preferred. Depending on the AFM cantilever, high torsional drive voltages may be needed. Due limitations of DACs, the system can only output in steps of 0.3 mV. Finer steps would not affect the output to the piezos.
- (h) Once both optimal conditions for force and torsional drive amplitude have been determined, open the frequency sweep again to confirm the resonance peak is selected. Then after returning from the sweep window, reduce the bandwidth to the most optimal.
- (i) The above protocol was used in main text Fig. 3 and has been shown. Now the scan area can be changed from many microns to many nanometers without changing anything more than scan speed and with it the bandwidth. The torsional drive amplitude and force do not have to be changed, for this region.
- (j) Some additional optimizations are mentioned after the note on imaging atomic lattices.

3. Imaging atomic lattices.

- (a) An example of imaging conditions for atomic lattices is shown in Fig. S10 (B).

A Scan Settings for tBG Moiré Superlattice			B Scan Settings for hBN Atomic Lattice		
<input checked="" type="checkbox"/>	Scan				
<input checked="" type="checkbox"/>	Scan Size	75.0 nm			
<input checked="" type="checkbox"/>	Aspect Ratio	1.00			
<input checked="" type="checkbox"/>	X Offset	16.850 μ m			
<input checked="" type="checkbox"/>	Y Offset	4.103 μ m			
<input checked="" type="checkbox"/>	XY Move Tip Pos	Retract			
<input checked="" type="checkbox"/>	Scan Angle	90.0 °			
<input checked="" type="checkbox"/>	Scan Rate	4.07 Hz			
<input checked="" type="checkbox"/>	Tip Velocity	0.763 μ m/s			
<input checked="" type="checkbox"/>	Zoom in at Constant	Scan Rate			
<input checked="" type="checkbox"/>	Samples/Line	512			
<input checked="" type="checkbox"/>	Lines	512			
<input checked="" type="checkbox"/>	Slow Scan Axis	Enabled			
<input type="checkbox"/>	Scan Single Frame Number	1			
<input type="checkbox"/>	Idle Depolarize Threshold	5 %			
<input type="checkbox"/>	Idle Depolarize Warning Tin	7200 s			
<input type="checkbox"/>	Idle Depolarize Withdraw Ti	18000 s			
<input checked="" type="checkbox"/>	Rounding	0.200			
<input type="checkbox"/>	Auto Adjust Rounding	No			
<input checked="" type="checkbox"/>	XY Closed Loop	Off			
<input checked="" type="checkbox"/>	Bidirectional Scan	Disabled			
<input checked="" type="checkbox"/>	Feedback				
<input checked="" type="checkbox"/>	SPM Feedback	TR Deflection			
<input checked="" type="checkbox"/>	Lock-In1 / DDS1	Enabled			
<input checked="" type="checkbox"/>	Lateral 16x Gain	Disabled			
<input checked="" type="checkbox"/>	Integral Gain	1.000			
<input checked="" type="checkbox"/>	Proportional Gain	2.000			
<input checked="" type="checkbox"/>	Analog2	0 V			
<input checked="" type="checkbox"/>	Analog4	0 V			
<input checked="" type="checkbox"/>	Drive DC Offset	0 V			
<input checked="" type="checkbox"/>	LP Vertical Deflection	10.00 kHz			
<input checked="" type="checkbox"/>	Reference Frequency	1456.828 kHz			
<input checked="" type="checkbox"/>	Setpoint Units	Volts			
<input checked="" type="checkbox"/>	Z Slew Rate Limit	0.00 μ m/s			
<input checked="" type="checkbox"/>	Torsion				
<input checked="" type="checkbox"/>	TR Mode	Enabled			
<input checked="" type="checkbox"/>	TR Deflection Setpoint	0.9700 V			
<input checked="" type="checkbox"/>	TR Drive Frequency	1456.828 kHz			
<input checked="" type="checkbox"/>	TR Drive Amplitude	2.500 mV			
<input checked="" type="checkbox"/>	TR Lock-In Phase	-38.44 °			
<input checked="" type="checkbox"/>	TR Lock-In BW	102.6 kHz			
<input checked="" type="checkbox"/>	TR Balance	0.03906 V			
<input checked="" type="checkbox"/>	Interleave				
<input checked="" type="checkbox"/>	Torsion (Interleave)				
<input checked="" type="checkbox"/>	Limits				
<input checked="" type="checkbox"/>	Z Limit	2.000 um			
<input checked="" type="checkbox"/>	Z Range	2.00 μ m			
<input checked="" type="checkbox"/>	Reduced Z Delay	2.00 s			
<input checked="" type="checkbox"/>	Z Auto Center Boundary	0 %			
<input checked="" type="checkbox"/>	Amplitude Range	1000 mV			
<input checked="" type="checkbox"/>	TR Amplitude Range	1000 mV			
<input checked="" type="checkbox"/>	Other				
<input checked="" type="checkbox"/>	FPGA Z Feedback	On			
<input checked="" type="checkbox"/>	Scan				
<input checked="" type="checkbox"/>	Scan Size	8.00 nm			
<input checked="" type="checkbox"/>	Aspect Ratio	1.00			
<input checked="" type="checkbox"/>	X Offset	0.000 nm			
<input checked="" type="checkbox"/>	Y Offset	0.000 nm			
<input checked="" type="checkbox"/>	XY Move Tip Pos	Retract			
<input checked="" type="checkbox"/>	Scan Angle	90.0 °			
<input checked="" type="checkbox"/>	Scan Rate	24.4 Hz			
<input checked="" type="checkbox"/>	Tip Velocity	0.488 μ m/s			
<input checked="" type="checkbox"/>	Zoom in at Constant	Scan Rate			
<input checked="" type="checkbox"/>	Samples/Line	1024			
<input checked="" type="checkbox"/>	Lines	1024			
<input checked="" type="checkbox"/>	Slow Scan Axis	Enabled			
<input type="checkbox"/>	Scan Single Frame Number	1			
<input type="checkbox"/>	Idle Depolarize Threshold	5 %			
<input type="checkbox"/>	Idle Depolarize Warning Tin	7200 s			
<input type="checkbox"/>	Idle Depolarize Withdraw Ti	18000 s			
<input checked="" type="checkbox"/>	Rounding	0.200			
<input type="checkbox"/>	Auto Adjust Rounding	No			
<input checked="" type="checkbox"/>	XY Closed Loop	Off			
<input checked="" type="checkbox"/>	Bidirectional Scan	Disabled			
<input checked="" type="checkbox"/>	Feedback				
<input checked="" type="checkbox"/>	SPM Feedback	TR Deflection			
<input checked="" type="checkbox"/>	Lock-In1 / DDS1	Enabled			
<input checked="" type="checkbox"/>	Lateral 16x Gain	Enabled			
<input checked="" type="checkbox"/>	Integral Gain	1.000			
<input checked="" type="checkbox"/>	Proportional Gain	2.000			
<input checked="" type="checkbox"/>	Analog2	0 V			
<input checked="" type="checkbox"/>	Analog4	0 V			
<input checked="" type="checkbox"/>	Drive DC Offset	0 V			
<input checked="" type="checkbox"/>	LP Vertical Deflection	10.00 kHz			
<input checked="" type="checkbox"/>	Reference Frequency	1428.286 kHz			
<input checked="" type="checkbox"/>	Setpoint Units	Volts			
<input checked="" type="checkbox"/>	Z Slew Rate Limit	0.00 μ m/s			
<input checked="" type="checkbox"/>	Torsion				
<input checked="" type="checkbox"/>	TR Mode	Enabled			
<input checked="" type="checkbox"/>	TR Deflection Setpoint	0.06000 V			
<input checked="" type="checkbox"/>	TR Drive Frequency	1428.286 kHz			
<input checked="" type="checkbox"/>	TR Drive Amplitude	2.500 mV			
<input checked="" type="checkbox"/>	TR Lock-In Phase	-76.98 °			
<input checked="" type="checkbox"/>	TR Lock-In BW	6.029 kHz			
<input checked="" type="checkbox"/>	TR Balance	0.03906 V			
<input checked="" type="checkbox"/>	Interleave				
<input checked="" type="checkbox"/>	Torsion (Interleave)				
<input checked="" type="checkbox"/>	Limits				
<input checked="" type="checkbox"/>	Z Limit	1.000 um			
<input checked="" type="checkbox"/>	Z Range	1.00 μ m			
<input checked="" type="checkbox"/>	Reduced Z Delay	2.00 s			
<input checked="" type="checkbox"/>	Z Auto Center Boundary	0 %			
<input checked="" type="checkbox"/>	Amplitude Range	1000 mV			
<input checked="" type="checkbox"/>	TR Amplitude Range	1000 mV			
<input checked="" type="checkbox"/>	Other				
<input checked="" type="checkbox"/>	FPGA Z Feedback	On			

FIG. S10. Imaging settings for moiré superlattices and atomic lattices (A) An example of settings to image a tBG moiré and (B) the atomic lattice of hBN are shown with the key parameters being force, shown by TR Deflection Setpoint represented in volts, torsional drive amplitude, shown by TR Drive Amplitude, in millivolts. The lock-in bandwidth for (A) is over 100 kHz as force and drive amplitude were changed to find the optimal settings for imaging and was reduced once ideal settings were found. Note the larger area image in (A) is taken at a line scan speed of 4.07 Hz while the relatively smaller image in (B) is taken at 24.4 Hz.

- (b) With the above complete, move into the R.O.I. where the atomic lattice has to be imaged.
- (c) With force set to about contact + 10 nN or contact + 20 nN, image over the region of interest and zoom into the about 5 to or 20 nm

square. The scan speed, points per line and lock-in bandwidth can all now be increased.

- (d) Then, lower the force to Contact + 0 nN and image the region.
- (e) Line scan speeds of 8-30 Hz were often used in conjunction with the lowest bandwidth, for

- that line scan speed, that did not show any signs of digitization in the line profile.
- (f) Points per line was increased to 512x512 typically.
 - (g) Step up the force in steps of 10 nN, with torsional drive amplitude set to between 2-5 mV, until an atomic lattice appears – in either amplitude or phase or both. For example, if the most recent “Last point of contact” was -0.1 V, then increase the force to -0.04V, +0.02V, +0.08V and so on. Sudden increases in force may damage both the AFM tip and sample as this is essentially a contact AFM technique. Ideal contrast should not require forces much greater than 50 nN for surfaces of hBN. Other materials may behave differently. VdW flake thickness may play another critical role and thinner flakes may show poorer contrast.
 - (h) Once the atomic lattice appears, open the sweep window again and tune to the peak of torsional resonance, again as it may have shifted with the increased force.
 - (i) Then, step through torsional drive amplitudes to further optimize contrast. Starting from about 1 mV, increase the drive amplitude in steps of 1 mV and observe the changes to the atomic lattice. The lowest torsional drive that yields the desired results is preferred. Depending on the AFM cantilever, high torsional drive voltages may be needed. Due limitations of DACs, the system can only output in steps of 0.3 mV. Finer steps would not affect the output to the piezos.
 - (j) Once both optimal conditions for force and torsional drive amplitude have been determined, open the frequency sweep again to confirm the resonance peak is selected. Then after returning from the sweep window, reduce the bandwidth to the most optimal.
 - (k) The above protocol was used in main text Fig. 2(B). Now the scan area can be changed from about 3 nm to 20 nm to while keeping the speed and bandwidth the same to confirm if the image represents an atomic lattice and not periodic noise. The torsional drive amplitude and force do not have to be changed.
 - (l) Some additional optimizations are mentioned below.
4. Some common suggestions applicable to both moiré superlattice and atomic lattice imaging.
- (a) Lower the gain to value like 1(I) and 2(P), when imaging over a smooth surface. If the gain is high, ringing would be apparent in the TR Deflection Error channel.
 - (b) The scan angle can be changed from 0° to 90° or other values.
 - (c) The parameter of “Rounding” set to 0.2 for scans about 100nm or smaller in open loop X-Y mode enables scanning 10% excess on either side of the fast scan axis and may help remove artifact at the edges of the scan frame.
 - (d) To optimize imaging, the “Lateral 16x gain” from the feedback category can be enabled. This only amplifies the TR amplitude and not the phase.
 - (e) Alternatively, if the signal is fairly large already (over 100 mV), then the “TR Amplitude Range” and “Amplitude Range” can be reduced from 4000 mV to a lower value. At a range of 4000 mV, the lock-in is configured to take in an input of \pm 2000 mV. For a 100 mV signal if 16x gain is turned on, that makes the signal 1600 mV and hence the full 4000 mV range of lock-in would be required. Conversely, if the signals are lower, the lock-in range can be reduced to increase sensitivity.
 - (f) Remember to save the data!
 - (g) Determine “Contact + 0 nN” every 30-120 minutes to ensure only the desired force is being applied. If the drift is making the vertical deflection shift to a more negative value, the force during imaging, is unintentionally and uncontrollably increasing (even though the feedback loop is operational to maintain the deflection setpoint) and could damage the sample.
 - (h) If both trace and retrace are being saved, the height sensor and TR deflection error channels can now be used to record the X-Y sensor data for the other pair of TR amplitude and phase.
5. Ending the imaging session.
- (a) When the image session is coming to an end, it is important to record certain parameters so that the instrument drift (and hence drift in the force applied) can be quantified.
 - (b) Upon clicking “Withdraw”, make a logbook entry.
 - (c) Move back to check parameters and make another logbook entry. Note the presence of the sample right below the AFM tip could affect the values measured and logging these values now would aid in determining the same.
 - (d) Next, move to navigate and move the sample to loading position.

- (e) Once the sample is not under the tip anymore, move to setup and make a logbook entry. Any change in value since the last recorded value is due to the presence of the sample in the vicinity. The change from when the laser was first aligned to this final logbook entry, tells the extent of drift in the force, if purely nominal force values were chosen by entering deflection in nanometers with respect to the original set-point of 0,0V. We found that forces in excess of 100 nN can be applied, unintentionally over a course of a few hours, if not logged accurately.

Note: The experiment can again be saved, but should be saved with a different name as the conditions saved would now be for imaging and not for instrument initialization. Initializing the instrument with these settings where the Z range may have been lowered, could be dangerous.

Image analysis (Optional)

1. Images presented in this work were analyzed in Gwyddion.

Note: Software bug: As of this writing, when .spm files from TFM (torsional resonance mode of the instrument) are opened in Gwyddion, the Z axis values are changed from indicating mV for amplitude and degrees ($^{\circ}$) for phase to showing volts (V). By analyzing the Z-scale of the data in NanoScope Analysis version 3.0, we confirmed that only the displayed units of volts are incorrect and can be swapped with mV and degrees in postprocessing.

2. The data was first corrected using the align rows function followed by fixing zero to the bottom of the scale.
3. Atomic lattice images could best be represented in an adaptive color scale (due to their relatively low contrast) while moiré superlattice images could be represented in all color scales (typically the linear scale was chosen).
4. 2D FFT analysis was also performed using the in-built functions to measure the lattice.
5. X-Y sensor-based postprocessing to correct for scanner piezo creep and hysteresis was not employed in this work. Coupled with thermal drift, piezo creep and hysteresis introduces uncertainty in precise determination of moiré period, twist angle and strain as well as angular orientation of atomic lattices.